JOURNAL OF PETROLOGY | VOLUME 49 | NUMBER 9 | PAGES 1549–1577 | 2008 | doi:10.1093/petrology/egn037

The Magmatic and Fluid Evolution of the Motzfeldt Intrusion in South Greenland: Insights into the Formation of Agpaitic and Miaskitic Rocks

JOHANNES SCHÖNENBERGER AND GREGOR MARKL*

INSTITUT FÜR GEOWISSENSCHAFTEN, AB MINERALOGIE UND GEODYNAMIK, EBERHARD-KARLS-UNIVERSITÄT, WILHELMSTRASSE 56, 72074 TÜBINGEN, GERMANY

RECEIVED JANUARY 29, 2008; ACCEPTED JULY 9, 2008
ADVANCE ACCESS PUBLICATION AUGUST 2, 2008

The 1·275 Ga Motzfeldt intrusive complex in the Gardar failed-rift Province in South Greenland formed from six successively intruding melt batches (SM1–SM6) interpreted to be derived from a common magma source at depth. Five units (SM1–SM5) crystallized an alkaline to peralkaline, miaskitic mineral assemblage of amphibole, clinopyroxene, feldspar, nepheline, Fe–Ti oxides, zircon, apatite, fluorite and rarely olivine. The last magmatic batch (SM6) is characterized by an agpaitic mineral assemblage of aegirine, nepheline, alkali-feldspar, eudialyte and rare fluorite or sodalite. Coexisting mafic minerals constrain the crystallization conditions of the miaskitic rocks to about 850–600°C, whereas solidus temperatures below 500°C are indicated by coexisting alkali feldspars in the agpaitic rocks. Oxygen fugacities during the orthomagmatic stage are below the FMQ (fayalite–magnetite–quartz) buffer (ΔFMQ −0·5 to −2·0) whereas late hematite provides evidence of a higher relative oxygen fugacity during late-stage alteration. The Nd and oxygen isotope compositions of amphiboles and pyroxenes are homogeneous throughout the complex and suggest a common, mantle-derived magma source for all six units which is comparable with other Gardar intrusions. The hydrogen isotopic composition of amphiboles (δD −99 to −132‰) indicates low-temperature fluid–rock interaction with low fluid–rock ratios. Fluid inclusion studies indicate that H_2O–NaCl fluids present during the magmatic stages in the miaskitic units had salinities of <10 wt % NaCl eq. Calcite crystals in fluid inclusions within these rocks suggest that CO_2 or HCO_3^- was an important component of the original fluid phase. In contrast, the agpaitic unit is characterized by a CH_4–H_2O–NaCl fluid. The C–O–H isotope compositions of the fluid inclusions in all units are consistent with mixing between a small volume of magmatic fluid and a large volume of meteoric water. The chemical evolution of the Motzfeldt complex is a type example of the connection of the transition from miaskitic to agpaitic mineral assemblages with redox-dependent fluid–solid equilibria. The transition from a relatively oxidized to a relatively reduced fluid is correlated with a change from a more reduced, Fe^{2+}-bearing miaskitic (taramite–arfvedsonite, zircon, SM1–SM5) to a more oxidized, Fe^{3+}-bearing agpaitic assemblage (aegirine, eudialyte, SM6). We suggest that coupled fluid–solid redox equilibria involving Fe^{2+}, Fe^{3+}, CO_2 and CH_4 in this case were simply driven by temperature decrease and an overall increase in Na (+K) in the melt. This observation sheds light on the heavily debated miaskite–agpaite transition. The combined temperature and compositional effect stabilized Fe^{3+}, CH_4 and enhanced the solubility of Zr (possibly as Na–Zr–Si–O complexes) in the latest stage melt (SM6) resulting in the crystallization of an agpaitic mineral assemblage. In terms of redox conditions during crystallization, the Motzfeldt rocks represent an intermediate case in the Gardar Province between more oxidized, CO_2-dominated intrusions such as the syenite–carbonatite complex of Grønnedal-Ika and CH_4-dominated, more reduced complexes such as the peralkaline granitic Puklen and the agpaitic Ilímaussaq complex.

KEY WORDS: *agpaite; methane; miaskite; nepheline syenite; redox reactions*

INTRODUCTION

Agpaitic rocks are peralkaline nepheline syenites that are characterized by the occurrence of complex Na–Zr silicates such as eudialyte instead of the more common

*Corresponding author. Telephone: +49 (0)7071 29 72930. Fax: +49 (0)7071 29 3060. E-mail: markl@uni-tuebingen.de

zircon and Fe–Ti oxides in miaskitic rocks (Sørensen, 1997). They represent some of the most highly differentiated magmatic rocks worldwide, sometimes exhibiting enrichments of high field strength elements (HFSE) such as Nb, Ta, U, Th, REE or Zr up to economic values (Sørensen, 1997). They occur as large intrusions (Ilímaussaq: Larsen & Sørensen, 1987; Markl *et al.*, 2001; Khibina and Lovozero: Kramm & Kogarko, 1994; Zaitsev *et al.*, 1998), as smaller parts of intrusions (Motzfeldt and Qoroq: Jones, 1980, 1984; Coulson, 1997; Mont St. Hilaire: Horvath & Gault, 1990; Tamazeght: Bouabdli *et al.*, 1988; Marks *et al.*, 2008) or as late-magmatic pegmatites (Crazy Mountains: Chakhmouradian & Mitchell, 2002; Oslo Rift: Brøgger, 1890, Fitou: Vitrac-Michard *et al.*, 1977; Gardiner Complex: Nielsen, 1994).

The petrogenesis of agpaitic rocks is not yet fully understood; however, they clearly originate from extensively differentiated, alkalic, mantle-derived mafic magmas (alkali basalts, nephelinites or benmoreites: Kramm & Kogarko, 1994; Sørensen, 1997). They show particularly long crystallization intervals down to temperatures <450°C (Piotrowski & Edgar, 1970; Sood & Edgar, 1970; Kogarko, 1977, 1987; Kogarko *et al.*, 1977; Larsen & Sørensen, 1987; Wolff, 1987) and can exhibit unusual melt immiscibility phenomena (Markl, 2001). The physico-chemical processes responsible for the formation of agpaitic mineral assemblages are not quantitatively understood and remain controversial. Markl *et al.* (2001) suggested and Krumrei *et al.* (2007) provided evidence for the existence of a very reduced, methane-rich fluid phase at high, orthomagmatic temperatures. Both the high alkali content of the rocks and the low water activity (methane-forming reaction consumes water: $CO_2 + 2H_2O = CH_4 + 2O_2$) would effectively prevent unmixing of an NaCl-rich hydrous fluid phase. Accordingly, Kogarko (1974), Kogarko & Romanchev (1983), Wallace *et al.* (1990) and Sørensen (1997) argued that HFSE and volatile elements are kept in the melt, which then gradually evolves towards silica-rich sodic aqueous solutions. Therefore, the melt would become highly enriched in alkalis and halogens compared with the differentiation products of similar parental magma compositions that exsolve a fluid phase at an earlier stage. This could be a prerequisite for the enrichment of HFSE complexed by halogens and for the formation of Na–HFSE–(halogen) minerals such as eudialyte.

Reduced conditions seem to be important for the evolution of strongly peralkaline and especially agpaitic rocks as evidenced by the studies of Konnerup-Madsen & Rose-Hansen (1982, 1984), Markl *et al.* (2001), Ryabchikov & Kogarko (2006), and Krumrei *et al.* (2007). In particular, the evolution and influence of a CH_4-bearing fluid phase seems to be of major significance (e.g. Markl *et al.*, 2001; Nivin *et al.*, 2001, 2002, 2005; Potter *et al.*, 2004; Beeskow *et al.*, 2006; Ryabchikov & Kogarko, 2006; Salvi & Williams-Jones, 2006; Krumrei *et al.*, 2007). Several hypotheses for methane formation in peralkaline intrusive rocks have been suggested: (1) primary magmatic methane (e.g. Markl *et al.*, 2001; Krumrei *et al.*, 2007); (2) late-magmatic reduction of a CO_2–H_2O-rich primary fluid as a result of closed-system cooling (e.g. Petersilie & Sørensen, 1970; Konnerup-Madsen & Rose Hansen, 1982; Konnerup-Madsen, 2001; Ryabchikov & Kogarko, 2006); (3) late- to post-magmatic Fischer-Tropsch-type reactions (Salvi & Williams-Jones, 1997; Potter & Konnerup-Madsen, 2003; Potter *et al.*, 2004). In all these scenarios, the redox reaction

$$CO_2 + 2H_2O = CH_4 + 2O_2 \quad (1)$$

plays a key role. Investigations of the redox conditions during the crystallization of peralkaline magmas are clearly crucial for understanding the details of the processes mentioned above.

In this respect, it is particularly useful to study the Motzfeldt intrusion in the Gardar Province of South Greenland, as its petrology is well known from the work of Jones (1980, 1984) and Jones & Larsen (1985) and it shows a transition from miaskitic to agpaitic rocks. We will show that the formation of agpaitic rocks in the Motzfeldt complex is a strong function of redox conditions.

REGIONAL GEOLOGY

The Gardar Province is a failed rift within which magmatic activity lasted from *c.* 1350 to 1120 Ma (Upton *et al.*, 2003). It is characterized by 12 major intrusions (Fig. 1), which comprise carbonatites, gabbros, granites and nepheline syenites. Several intrusions including Ilímaussaq, Motzfeldt and Qoroq contain agpaitic nepheline syenites with eudialyte and other complex Na–Zr–Ti silicates instead of miaskitic zircon and Fe–Ti oxides. Numerous dyke swarms presumably served as feeders for extensive regional volcanism evidenced by the basalts of the Eriksfjord Formation (Escher & Watt, 1970; Upton *et al.*, 2003) which also includes quartzitic sandstones.

The 1·275 Ga Motzfeldt intrusion (Upton *et al.*, 2003) forms part of the large Igaliko complex, which also includes the Qoroq and Igdlerfigssalik intrusions (Emeleus & Harry, 1970, Fig. 1). It intruded the Julianehåb batholith of the 1·8 Ga Ketilidian orogen (Garde *et al.*, 2002) at a depth of *c.* 4–6 km (Jones, 1980). The Motzfeldt intrusion mainly comprises nepheline syenites in which a number of several hundred metre long rafts of Eriksfjord basalts are embedded (Fig. 1). The intrusion was first mapped by Emeleus & Harry (1970). Jones (1980) provided a detailed petrological investigation of the intrusive units SM1–SM6, which he defined based on cross-cutting relationships in the field (Fig. 1). The whole-rock geochemistry and mineralogy of the main rock-forming minerals were studied in detail by Jones (1980, 1984), Jones & Peckett (1980), Jones & Larsen (1985), and Bradshaw (1988). The complex attracted economic interest during the Syduran

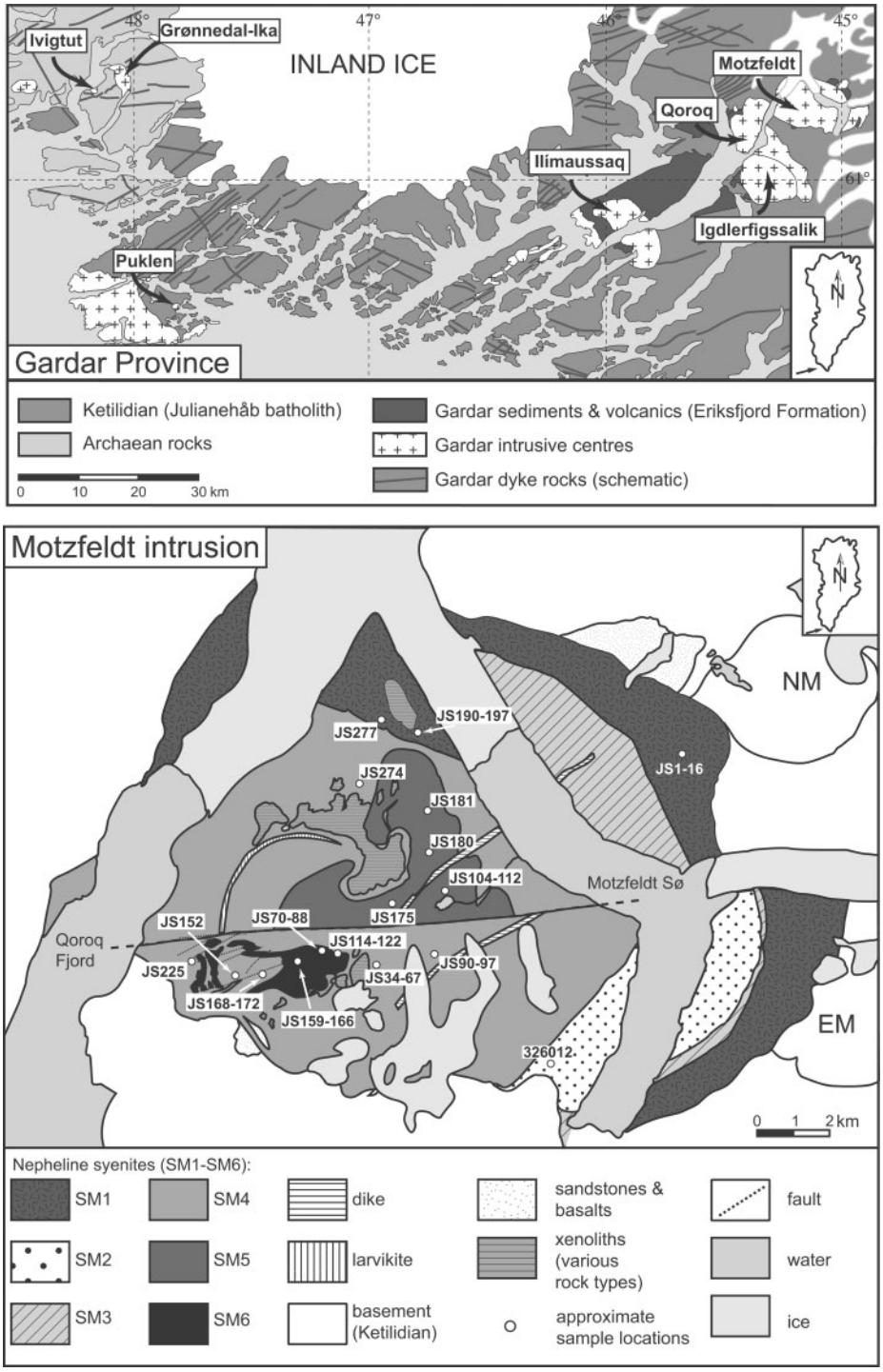

Fig. 1. Top: geological overview of the Gardar Province (modified after Upton & Emeleus, 1987). Bottom: geological map of the Motzfeldt intrusion (modified after Emeleus & Harry, 1970; Jones, 1980). NM and EM are North Motzfeldt and East Motzfeldt satellite intrusions.

project (Armour-Brown *et al.*, 1983; Tukiainen *et al.*, 1984) when considerable amounts of Nb were discovered, especially in the NE part of the intrusion in unit SM1. In this paper we use the SM1–SM6 nomenclature of Emeleus & Harry (1970) and Jones (1980) instead of the more complex one proposed by Tukiainen *et al.* (1984) as this is better suited for addressing the transition from miaskitic to agpaitic rocks. Furthermore, it is easier to compare our data with the earlier data of Jones (1980, 1984), Jones & Peckett (1980) and Jones & Larsen (1985).

PETROGRAPHY

Samples from units SM1, SM2, SM4, SM5 and SM6 (Table 1) were studied. In general, these rocks are miaskitic to agpaitic (± nepheline) syenites, interpreted to have originated from different magma batches (Jones, 1980). Detailed petrographic descriptions have been given by Jones (1980, 1984) and we summarize here only the most important information necessary to support our line of argument.

Miaskitic units SM1–SM5

The miaskitic units SM1, SM2, SM4 and SM5 are very uniform in terms of their mineral assemblages, but they vary in modal composition and grain size. Rock-forming minerals are amphibole, clinopyroxene, feldspar, nepheline, Fe–Ti oxides and accessory zircon, apatite, aenigmatite and pyrochlore (Jones, 1984).

Unit SM1 consists of <1 cm size grains, nepheline is absent and pyroxene is rare in the investigated samples. However, Jones (1980) described nepheline- and/or pyroxene-bearing varieties. Some samples contain primary magmatic fluorite (JS190, JS195, JS197; Schönenberger *et al.*, 2008). SM2 (only one sample, 326012, provided by H. Emeleus) consists of large, turbid feldspar laths (Fig. 2a) with interstitial brownish amphibole. The samples from unit SM4 (JS36, JS97, JS171, JS172) are relatively fine-grained (grain size <0·5 cm). Amphibole is occasionally poikilitic (Fig. 2d). Rinkite occurs intergrown with Fe–Ti oxides (Fig. 2e). The minerals in SM5 (Table 1) are much coarser (<2 cm) than in the other units. Feldspar characteristically forms laths several centimetres long. Occasionally, colourless to slightly green clinopyroxene occurs as cores within brown amphibole (Fig. 2h). Rare sodalite forms interstitial grains.

Alteration phenomena include the common turbidity of feldspars and replacement of amphibole by green pyroxene especially in units SM1, SM2 and SM5. SM1 is the most altered unit. Secondary minerals such as biotite, fluorite, quartz, titanite, and hematite are common. Calcite and cancrinite occur mainly as alteration products of nepheline, but also of feldspars in all units. Furthermore, calcite was observed in thin veinlets cutting all other rock types. Secondary veins consist of fluorite and/or quartz (SM1), fluorite ± calcite, ± aegirine (SM4) and fluorite ± feldspar (SM5). The unusual occurrence of quartz may be attributed to the assimilation of rafts of the Eriksfjord formation, which contain large amounts of quartzitic sandstone.

Agpaitic unit SM6

The samples of unit SM6 (Table 1) are dominated by green, euhedral to hypidiomorphic clinopyroxene, large euhedral nepheline and feldspar laths together with interstitial nepheline, eudialyte and minor amounts of fluorite and sodalite (Fig. 3). Amphibole is rare (Jones, 1980, 1984) and does not occur at all in the studied samples. The nepheline syenitic rocks of unit SM6 are called 'lujavrites'

Table 1: Investigated samples indicating the type of analyses performed

	SM1											SM2	SM4									
JS:	1	3	6	9	10	16	190	195	196	197	277	326012	34	36	67	90	91	97	152	168	171	172
m	x	x						x	x	x		x		x				x			x	x
sep									x	x		x									x	x
fl			x	x	x	x	x			x	x		x			x	x		x	x	x	x
flis			x	x		x											x					
IC			x	x		x					x								x	x		
CC															x							

	SM4		SM5									SM6										
JS:	225	274	104	105	108	109	110	112	175	180	181	70	88	114	122	159	162	163	164	165	166	
m				x	x			x		x	x	x		x		x	x	x	x	x	x	
sep					x					x		x		x		x						
fl	x	x	x		x	x	x		x	x			x		x							
flis	x	x				x			x						x							
IC	x	x				x			x													
CC						x					x					x			x			

M, microprobe; sep, O, H and Sm/Nd isotopes from mineral separates; fl, fluid inclusion analysis; flis, fluid isotopes; IC, ion chromatography; CC, carbonate isotopes.

based on their textural similarity to rocks from the Kola peninsula, Russia, and the Ilímaussaq intrusion in the Gardar Province. Magmatic modal layering is common and three distinct varieties of rocks can be defined: white (feldspar-dominated), green (pyroxene- and nepheline-dominated) and black (pyroxene-dominated) lujavrite (see Jones, 1980, 1984). The eudialyte in these rocks is especially heavily altered to complex REE-bearing phases

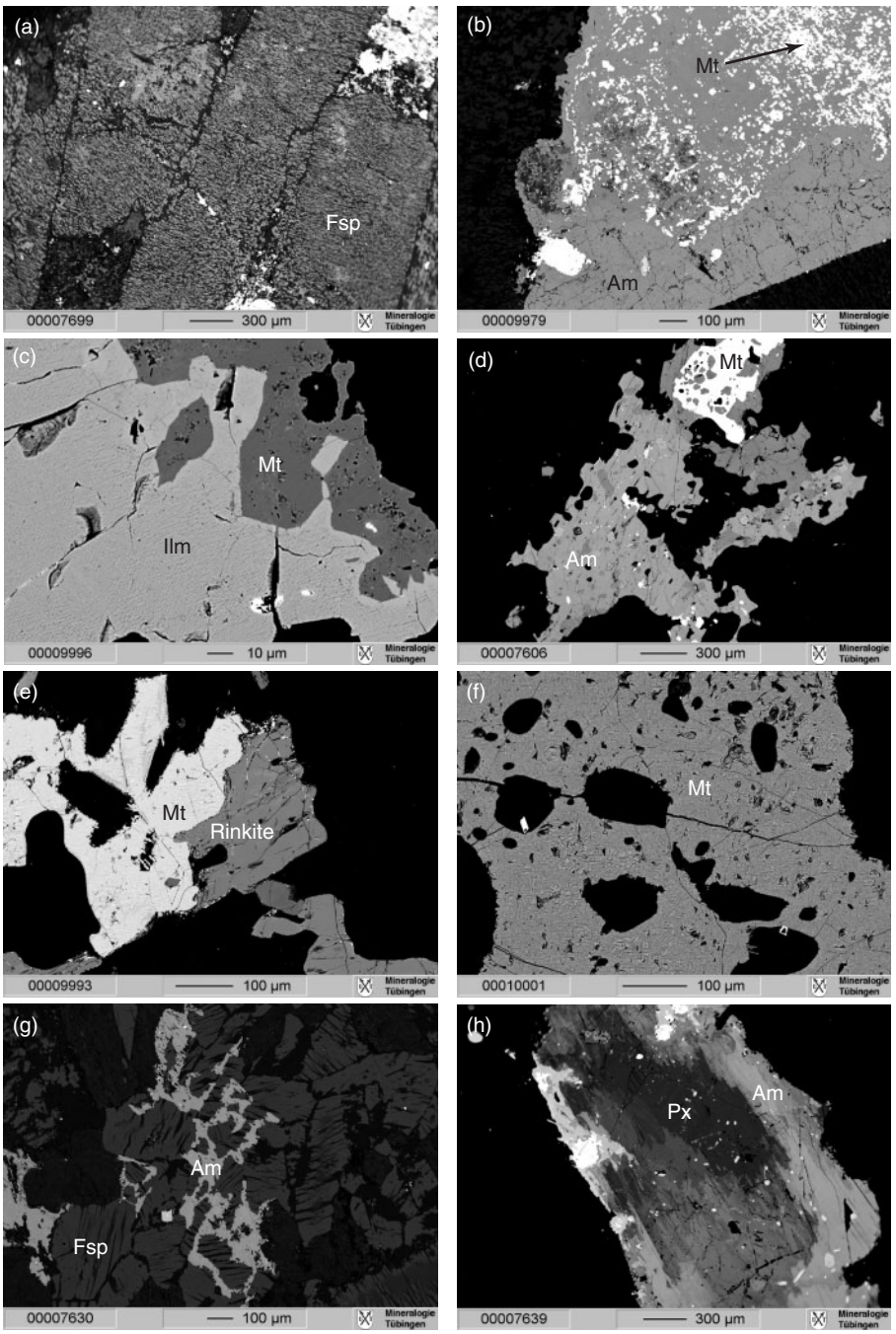

Fig. 2. Textures observed in the miaskitic units [back-scattered electron (BSE) images]. (a) Heterogeneously exsolved alkali feldspars in SM2 (326012). (b) Amphibole in unit SM1. It is altered to secondary amphibole with magnetite intergrowths. (c) Ilmenite and magnetite of SM1 (JS196) interpreted to have crystallized simultaneously. (d) Amphibole of SM4 (JS97) with inclusions of pyroxene and magnetite. (e) Magnetite and rinkite intergrown in unit SM4 (JS172). (f) Finely exsolved magnetite of SM4 (JS171). (g) Typical amphibole–feldspar association in SM4 (JS36). (h) Complex pyroxene–amphibole texture from SM5 (JS108) where a core of primary pyroxene is rimmed by secondary amphibole.

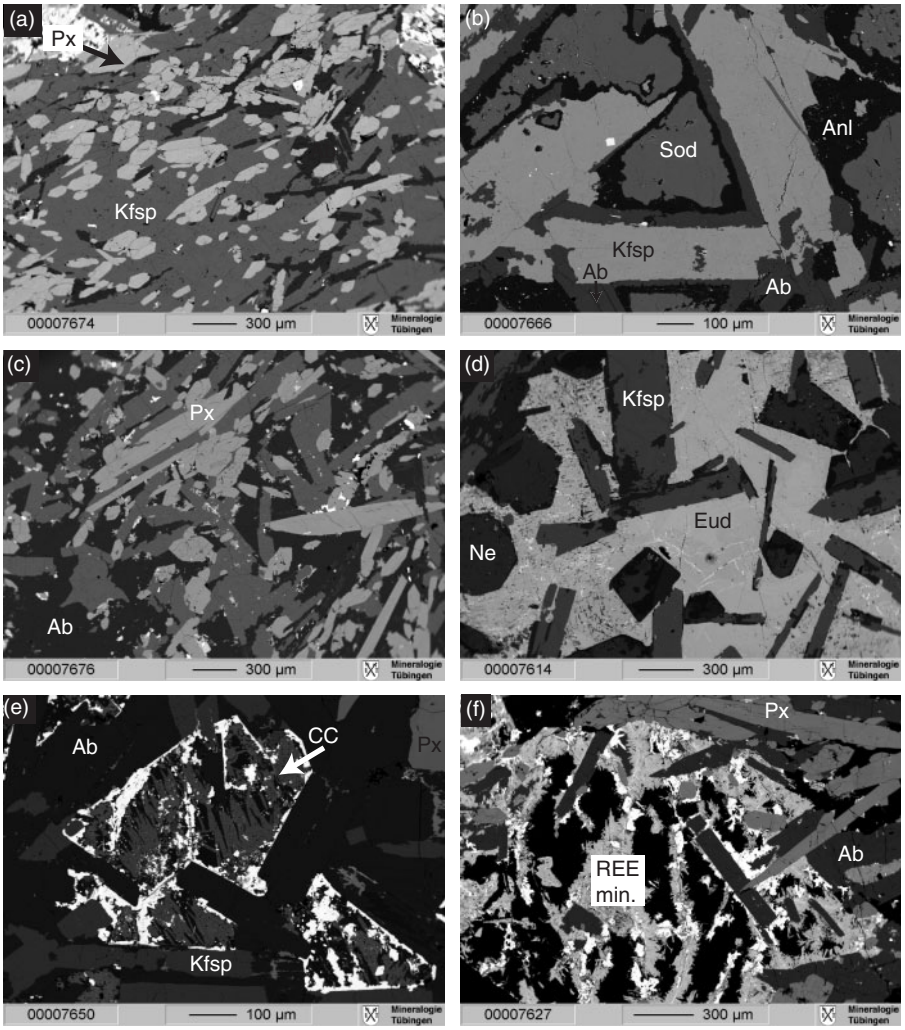

Fig. 3. Textures in the agpaitic unit SM6 (BSE images). (a) Typical texture of SM6 with euhedral pyroxenes and albite laths in a matrix of K-feldspar. (b) Large K-feldspar laths rimmed by albite and interstitial sodalite with analcite reaction rim. (c) Euhedral pyroxenes with K-feldspar laths in an albite matrix. (d) Poikilitic eudialyte enclosing slightly altered K-feldspar and nepheline. (e) Typical alteration texture of what may have been eudialyte comprising calcite (CC), albite, zircon and other REE-bearing minerals (bright colours). (f) Complex alteration texture where eudialyte is altered to secondary, complex trace element-rich minerals (REE-min.) together with analcite (black).

(Fig. 3). Alteration products are cancrinite, zircon, calcite, pectolite and trace element (REE)-rich minerals such as catapleiite, zirfesite, pyrochlore and others (Jones, 1980; Jones & Larsen, 1985). Comparable alteration phenomena were investigated in detail in the nearby Qoroq intrusion (Coulson, 1997).

ANALYTICAL METHODS

All analyses were carried out at the Institut für Geowissenschaften, Universität Tübingen, Germany. A JEOL 8900 electron microprobe was used for analysing minerals for their major element contents. It was calibrated using natural and synthetic standards. The beam current was 15 nA and acceleration voltage 15 kV. Counting time on the peak positions ranged between 16 s for major elements and 60 s for minor elements, and background counting times were half the peak time. A focused electron beam was used; however, Fe–Ti oxides, feldspar and nepheline were analyzed with a defocused beam (up to 20 µm beam diameter) to avoid alkali migration and/or to obtain average compositions. The overlap of F Kα and Fe Lβ peaks was corrected and an internal $\varphi\rho Z$ correction (Armstrong, 1991) was applied. Analytical uncertainties are below 1% (relative) for major elements, and up to around 5% (relative) for minor elements.

Details of the oxygen isotope analysis techniques for *c.* 10 mg handpicked pyroxene and amphibole mineral

separates have been given by Marks *et al.* (2003), who followed the methods of Sharp (1990) and Rumble & Hoering (1994). The determination of the hydrogen isotopic composition of *c.* 50 mg amphibole mineral separates was performed according to the method of Vennemann & O'Neil (1993). Oxygen and hydrogen isotopic compositions were analyzed on a Finnigan MAT 252 mass spectrometer. The analytical precision of the oxygen isotope analyses of the standards (NBS-28 quartz; Valley *et al.*, 1995) is ±0·1‰ and the precision of the in-house kaolinite standard for hydrogen isotope analyses is ±2‰. All stable isotope analyses in this study are reported in permil (‰) in standard notation relative to VSMOW (oxygen and hydrogen) and VPDB (carbon).

Detailed description of the analyses of the Nd isotopic compositions of ~10 mg of hand-picked mineral separates have been given by Marks *et al.* (2003). After spiking with a ^{150}Nd–^{149}Sm tracer, the samples were dissolved in HF at 180°C in poly-tetrafluor-ethylene (PTFE) reaction bombs. Sm and Nd were separated in quartz columns using 1·7 ml Teflon powder coated with HDEHP (di-ethyl hexyl phosphate) for cation exchange. A Finnigan MAT262 thermal ionization mass spectrometer was used. Analyses of the LaJolla standard yielded a $^{143}Nd/^{144}Nd$ ratio of 0·511824 ± 10 (±2σ error, $n = 13$). The blank of the total procedure (chemistry and loading) was <100 pg for Nd. The decay constant of Lugmair & Marti (1978) was used for ^{147}Sm ($6{\cdot}54 \times 10^{-12}$ a^{-1}). Present-day CHUR values of 0·1967 ($^{147}Sm/^{144}Nd$; Jacobson & Wasserburg, 1980) and 0·512638 ($^{143}Nd/^{144}Nd$; Goldstein *et al.*, 1984) were applied to calculate $\varepsilon_{Nd}(t)$ values. Initial Nd isotope ratios were corrected for an age of 1·275 Ga (Upton *et al.*, 2003; J. McCreath, unpublished data). The uncertainty in $\varepsilon_{Nd}(t)$ ratios is <0·5 based on analytical errors.

For fluid inclusion investigations, doubly polished, 100–300 μm thick wafers of nepheline, fluorite, feldspar and quartz were analyzed using a Leica DMLP microscope and a Linkam THMS 600 heating–cooling stage for fluid petrography and microthermometry. The heating–cooling stage was calibrated using synthetic CO_2 and H_2O standards. The accuracy of melting and homogenization temperatures is ±0·2 and ±2·0°C, respectively. Raman spectroscopy was performed using a Dilor Jobin Yvor Raman spectroscope. Fluid inclusions and the mineral matrix were analyzed using a blue argon laser (488 nm) for a wave number range between 600 and 4500 cm^{-1}. Counting times varied between 10 and 60 s.

The bulk chemistry of the fluid inclusions was determined using a Dionex ICS1000 ion chromatography system with a CS-12A cation column and an AS9-HC anion column. All samples were treated with concentrated (65%) HNO_3 at 60–70°C in a sand bath for 4 h and washed with triple deionized water for 7 days to prevent any contamination from the HNO_3 washing procedure. After having ground 2 g of each sample in an agate mortar, the salts were dissolved in 10 ml triple deionized water. For anions, 5 ml were injected. To the remaining 5 ml, 10 μl of 33% HNO_3 were added to ensure a pH value between 2 and 3 required for the cation column. The run time of the samples was 30 min. Analytical errors are in the range of 20% relative (Köhler *et al.*, 2008).

Fluid inclusions in fluorite samples were analyzed for their C, H and O isotopic composition using the low-temperature crushing method described by Friedman (1953), Craig (1961) and Vennemann & O'Neil (1993). The samples were carefully hand-picked, dried and mechanically crushed. Fluorite, which was found to be finely intergrown with carbonate, was treated with concentrated HNO_3 prior to analysis to preclude any contamination effect on the fluid inclusion content. δD, $\delta^{18}O$ and $\delta^{13}C$ values of hydrocarbons, CO_2 and H_2O were measured on a Finnigan MAT-252 mass spectrometer. The analytical error is 0·3‰ for oxygen and carbon and better than 6‰ for hydrogen.

To analyze the isotopic composition of the calcite crystals trapped in fluid inclusions, one fluorite sample (JS109) was thoroughly washed with concentrated HCl to remove possible carbonate intergrowths. This sample was heated to 1000°C in the same analytical set-up as that used for the isotope analyses of the fluid inclusions to thermally decompose the calcite daughter crystals (e.g. Hollemann & Wiberg, 1995). The thermal decomposition of calcite proceeds according to the reaction $CaCO_3 \rightarrow CaO\ (solid) + CO_2\ (gas, measured)$; Hollemann & Wiberg, 1995). Significant fractionation of oxygen isotopes can be ruled out at the high temperatures used (*c.* 1000°C; e.g. Zheng, 1999).

The oxygen and carbon isotopic composition of carbonates were analyzed according to the method described by Spötl & Vennemann (2003), using a ThermoFinnigan GasBench connected directly to a Finnigan MAT 252 mass spectrometer. Orthophosphoric acid (100%) was added to <500 mg of carbonate powder or several grams of whole-rock powder to release the CO_2 from the sample. To remove water vapour and interfering gases, the CO_2 vapour was led via a He stream and a gas chromatograph column. Subsequently the CO_2 was passed into the mass spectrometer. The standard analytical errors are 0·1‰ for $\delta^{13}C$ and $\delta^{18}O$. As petrographic investigations showed that apart from carbonates, cancrinite may also be present in the samples, test measurements were performed to extract the CO_2 only from calcite and not from cancrinite. These measurements yielded excellent values for a reaction time of 85 min where >98 vol.% of calcite reacted whereas only minor amounts of CO_2 from cancrinite were detected (<2 vol.%).

RESULTS

Mineral chemistry

Electron microprobe analyses were carried out on minerals of units SM1, SM2, SM4, SM5 and SM6. Only a brief summary of the data is given here, as Jones (1980, 1984) has

already characterized the mineral chemistry of the intrusive phases in detail.

Amphibole

The composition of the amphiboles from units SM1–SM5 (Table 2) is mainly characterized by the exchange CaAl ↔ NaSi and ranges from Ca-dominated via Na–Ca- to Na-dominated compositions including taramite, katophorite, ferro-nyböite and arfvedsonite (Leake, 1997). Fe^{3+} is mostly below 1 a.p.f.u. The fluorine content is around 1 wt % (SM1, SM2, SM4) but is up to 3·5 wt % (=1·7 a.p.f.u.) in unit SM1. However, amphiboles from SM5 exhibit larger variations obeying the F–Fe avoidance rule (e.g. Marks *et al.*, 2003; Schönenberger *et al.*, 2006).

Clinopyroxene

The composition of the pyroxenes varies from diopside/hedenbergite-dominated pyroxenes via aegirine–augite to almost pure aegirine-endmember pyroxenes (Table 3, Fig. 4). The diopside/hedenbergite-rich pyroxenes mainly occur in SM4 and SM5 as cores that are overgrown by aegirine–augite. Jones (1980) also described such pyroxenes from units SM1 and SM2 (Fig. 4). Unit SM6 only crystallized almost pure aegirine. The jadeite content increases with increasing $NaFe^{3+}$ content, but does not exceed 8 mol %. ZrO_2 is up to 1·2 wt % in our samples, but has been reported to attain 6·96 wt % (Jones, 1980; Jones & Peckett, 1980).

Fe–Ti oxides

The Fe–Ti oxides from units SM1, SM4, SM5 and SM6 (Table 4) are titanomagnetites that are commonly heterogeneously exsolved to magnetite with lamellae of the hematite–ilmenite–pyrophanite solid solution series. In unit SM1, textures suggest that ilmenite ($Ilm_{77–85}Hm_{3–7}Pyr_{10–19}$) and titanomagnetite ($Mt_{56–74}Usp_{44–36}$) crystallized as (primarily) separate grains (Fig. 2). Finely exsolved titanomagnetite from SM4 (Fig. 2) shows reintegrated average compositions of $Mt_{69–78}Usp_{31–22}$. Reintegrated titanomagnetites from SM5 usually show compositions of $Mt_{50–56}Usp_{50–44}$ and a few compositions reach extreme values of $Mt_{37}Usp_{63}$. Magnetites occurring as alteration products of amphibole (e.g. sample JS180, SM5; but also in other samples from SM1 and SM4) commonly have a composition of $Mt_{>90}Usp_{<10}$. In SM6, no primary Fe–Ti oxide phase is present but almost pure hematite ($Hm_{94–99}Ilm_{0–5}Pyr_{0–2}$) occurs as an alteration product of aegirine.

Feldspars

Feldspars commonly exhibit coarse perthitic exsolution textures (Fig. 2, SM1–SM5). The composition of the reintegrated feldspar grains is: SM1 $Ab_{57–73}Or_{27–43}$; SM2 $Ab_{47–65}Or_{45–53}$; SM4 and SM5 $Ab_{37–52}Or_{48–63}$. This corresponds to an increase in the Or component from SM1 to SM5. The anorthite content of the feldspars is always $<An_1$. In SM6 two separate feldspars of almost endmember composition ($Ab_{>98}Or_{<2}$ and $Ab_{<5}Or_{>95}$) crystallized, as noted by Jones (1980) and Jones & Larsen (1985).

Nepheline

Because of the strong alteration of nepheline within our samples from units SM1 and SM2, nepheline was analyzed in units SM4–SM6 only. Its composition ranges from $Ne_{74}Ks_{16}Qz_{10}$ to $Ne_{76}Ks_{23·6}Qz_{0·4}$ (Fig. 5). Jones (1980) and Jones & Larsen (1985) reported nepheline from other units with similar compositions.

Isotopic composition of mineral separates

The isotopic composition (O, H, Nd, Table 5) of amphibole was determined from SM1 (JS195, 196), SM2 (326012), SM4 (JS171, JS172) and SM5 (JS108, JS181), and of pyroxenes from SM6 (JS70, JS114, JS159).

The $\delta^{18}O$ values range from +4·2 to +5·3‰ (VSMOW, Fig. 6). Samples from SM1 have the lowest values (+4·2 and +4·6‰). The δD of amphibole varies between −98 and −132‰ (VSMOW) with SM1 and SM2 having the lowest values of −120·1‰ (SM1), −127·6‰ (SM1) and −132·3‰ (SM2), respectively.

Initial $\varepsilon_{Nd}(t)$ values (t=1·275 Ga; Upton *et al.*, 2003; J. McCreath, personal communication, 2007) for the mineral separates range from +0·1 to +2·4. SM1 and SM2 have the lowest values whereas SM4 and SM5 have values similar to those for SM6 (+0·9 to +2·4, Fig. 6).

Carbon and oxygen isotope compositions of carbonates were analyzed for three whole-rocks from units SM5 and SM6 (JS159, JS164, JS181, Table 6) that contain finely disseminated calcite occurring as alteration products and/or in very small veinlets. $\delta^{13}C$ values range from −2·1 to −3·2‰ (VPDB, Fig. 7). The oxygen isotopic compositions of these samples varies from +21·9 to +24·2‰ ($\delta^{18}O$, VSMOW). Additionally, calcite from one calcite vein within SM4 (JS67, Table 6) yielded a $\delta^{13}C$ value of −4·4‰ (VPDB) and a $\delta^{18}O$ value of +7·8‰ (VSMOW). Calcite crystals from fluid inclusions analyzed in one sample (JS109, Table 6) have $\delta^{13}C$ and $\delta^{18}O$ values of −3.9‰ and +8.1‰, respectively.

Fluid inclusion investigations

Petrography and microthermometry

Fluid inclusions were analyzed from magmatic fluorites of SM1 (JS190, JS197) and SM6 (JS88, JS122; Schönenberger *et al.*, 2008) and magmatic nepheline and feldspar of SM4 and SM5 (JS171, JS172, JS104, JS108, JS180, Fig. 8). Hydrothermal fluorites were studied from units SM1, SM4 and SM5 (Table 1) and secondary hydrothermal quartz in unit SM1 (JS10, JS277). Four types of fluid inclusions can be distinguished: (1a) saline–aqueous two-phase (liquid–vapour; l–v) inclusions; (1b) saline–aqueous three-phase inclusions (liquid–vapour–solid; l–v–s); (2) pure CO_2 two-phase (liquid–vapour; l–v) inclusions (only in sample JS34); (3) aqueous–CH_4 one- or two-phase

Table 2: Representative microprobe analyses of Motzfeldt amphiboles

JS:	195	197	326012	97	171	105	108
Unit:	SM1	SM1	SM2	SM4	SM4	SM5	SM5
wt %							
SiO_2	43·86	47·56	39·30	41·96	42·50	44·02	45·14
TiO_2	1·81	0·99	1·55	1·69	1·38	2·78	1·77
Al_2O_3	5·54	3·00	8·68	6·78	6·01	7·04	5·21
FeO	27·91	27·39	31·59	31·09	28·86	19·02	22·87
MnO	1·06	1·12	1·51	1·44	1·68	0·94	1·46
MgO	4·23	5·17	1·11	1·36	3·01	9·14	7·03
CaO	6·89	3·59	8·57	7·21	6·99	9·97	7·68
Na_2O	5·10	6·90	4·05	4·72	5·00	3·76	5·05
K_2O	1·53	1·35	1·61	1·75	1·71	1·55	1·61
ZrO_2	0·32	0·33	0·36	0·29	0·32	0·12	0·38
Cl	0·00	0·03	0·05	0·01	0·02	0·02	0·01
F	0·98	1·65	0·23	0·18	0·68	1·74	1·28
Total	99·23	99·08	98·61	98·48	98·16	100·1	99·49
Formula based on 16 cations and 23 anions							
Si	6·90	7·42	6·33	6·73	6·79	6·72	6·96
Al	1·03	0·55	1·65	1·28	1·13	1·27	0·95
Ti	0·21	0·12	0·19	0·20	0·17	0·32	0·21
Fe^{3+}	0·55	0·67	0·85	0·63	0·81	0·04	0·48
Mg	0·99	1·20	0·27	0·32	0·72	2·08	1·62
Fe	3·12	2·90	3·40	3·55	3·04	2·39	2·47
Mn	0·14	0·15	0·21	0·20	0·23	0·12	0·19
Ca	1·16	0·60	1·48	1·24	1·20	1·63	1·27
Na	1·56	2·09	1·27	1·47	1·55	1·11	1·51
K	0·31	0·27	0·33	0·36	0·35	0·30	0·32
Zr	0·02	0·03	0·03	0·02	0·02	0·01	0·03
Cl	0·00	0·01	0·01	0·00	0·00	0·00	0·00
F	0·49	0·81	0·12	0·09	0·34	0·84	0·62
Sum	16·00	16·00	16·00	16·00	16·00	16·00	16·00

inclusions. The last fluid inclusion type is unique to the agpaitic unit SM6 whereas the first three types [(1a), (1b) and (2)] occur only in the miaskitic units SM1–SM5. Inclusions of type (1) also contain trace amounts of CO_2 and CH_4 (detected only during isotope analyses). For the saline–aqueous fluid inclusions, salinities (wt % NaCl eq.) were calculated according to Bodnar (1993; Table 7, Fig. 9).

(1a) *Saline–aqueous two-phase inclusions*. These fluid inclusions are the dominant type in the investigated samples. In primary magmatic fluorite of SM1 (Fig. 8a), they mainly occur along (pseudo)secondary trails, have an irregular to rounded shape and reach sizes up to 40 μm. They have salinities of <3·5 wt % NaCl eq. and filling ratios of 0·85–0·95. The fluid inclusions in magmatic nepheline (units SM4 and SM5) are rectangular and generally <20 μm in size. They show negative crystal shapes and occur as isolated inclusions or in groups but also in pseudo-secondary trails and have filling ratios between 0·80 and 0·95. The isolated fluid inclusions are interpreted to be of primary origin (Shepherd *et al.*, 1985). Fluid inclusions from primary magmatic minerals from SM4 (JS171, JS172) typically have salinities <2–5 wt % NaCl eq., but some reach 6–7 wt % NaCl eq. In nephelines from samples of SM5 (JS104, JS108, JS180), most fluid inclusions (80%) vary in salinity between 4 and 6 wt % NaCl eq.

Hydrothermally formed (secondary) fluorites of units SM1, SM4 and SM5 mainly contain trails of secondary fluid inclusions and only a few isolated ones. They are commonly of irregular shape, but also rounded to angular (Fig. 8b). The size of fluid inclusions varies from <5 μm to 100 μm (Fig. 8). Necking-down was occasionally observed but these fluid inclusions were not further analyzed.

Table 3: Representative microprobe analyses of Motzfeldt clinopyroxenes

JS:	1	326012	97	171	171	172	108	180	180	114	166
Unit:	SM1	SM2	SM4	SM4	SM4	SM4	SM5	SM5	SM5	SM6	SM6
wt %											
SiO_2	52·77	49·01	49·41	49·50	50·90	48·69	50·06	50·75	52·98	52·10	51·80
TiO_2	2·69	0·30	0·75	0·23	0·22	0·32	0·38	0·56	1·29	0·35	0·37
Al_2O_3	0·80	0·87	2·06	0·86	0·90	0·86	0·77	1·18	1·79	0·95	1·10
FeO	27·58	25·20	17·84	24·47	24·76	24·91	23·03	13·55	27·08	28·55	28·27
MnO	0·02	1·86	0·93	1·41	0·95	1·42	1·52	0·94	0·50	0·29	0·38
MgO	0·04	1·11	6·88	1·76	1·89	1·55	2·74	9·91	0·27	0·10	0·12
ZrO_2	0·06	0·31	0·09	0·37	0·41	0·31	0·88	0·12	0·15	0·72	0·42
CaO	0·04	18·17	22·17	15·56	9·87	18·10	16·62	22·49	0·67	1·79	2·22
Na_2O	13·91	2·82	0·71	4·68	8·26	3·22	3·69	0·95	13·44	12·79	12·58
Total	97·91	99·65	100·84	98·84	98·16	99·38	99·69	100·45	98·17	97·64	97·26
Formula based on 6 oxygens and 4 cations											
Si	1·99	1·97	1·91	1·96	1·97	1·95	1·98	1·92	1·99	1·99	1·98
Al	0·04	0·04	0·09	0·04	0·04	0·04	0·04	0·05	0·08	0·04	0·05
Ti	0·08	0·01	0·02	0·01	0·01	0·01	0·01	0·02	0·04	0·01	0·01
Cr	0·00	0·00	0·00	0·00	0·00	0·00	0·00	0·00	0·00	0·00	0·00
Fe^{3+}	0·85	0·23	0·10	0·38	0·62	0·30	0·27	0·14	0·85	0·91	0·90
Mg	0·00	0·07	0·40	0·10	0·11	0·09	0·16	0·56	0·02	0·01	0·01
Fe	0·02	0·62	0·48	0·43	0·18	0·53	0·49	0·29	0·01	0·00	0·01
Mn	0·00	0·06	0·03	0·05	0·03	0·05	0·05	0·03	0·02	0·01	0·01
Zr	0·00	0·01	0·00	0·01	0·01	0·01	0·02	0·00	0·00	0·01	0·01
Ca	0·00	0·78	0·92	0·66	0·41	0·77	0·70	0·91	0·03	0·07	0·09
Na	1·02	0·22	0·05	0·36	0·62	0·25	0·28	0·07	0·98	0·95	0·93
Sum	4·00	4·00	4·00	4·00	4·00	4·00	4·00	4·00	4·00	4·00	4·00

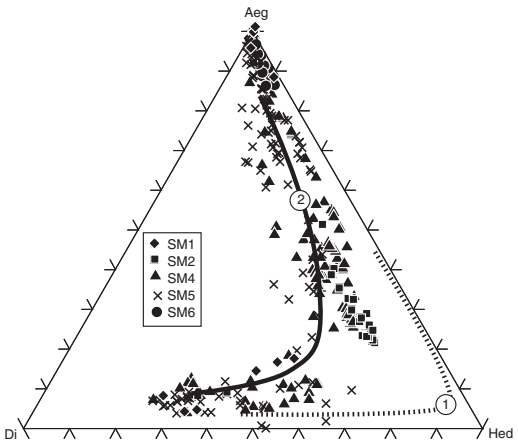

Fig. 4. Evolution of pyroxene composition in the diopside–hedenbergite–aegirine triangle [data from this study and Jones (1980)]. For comparison, dotted curve 1 is general trend of clinopyroxene evolution in the Ilímaussaq intrusion (Larsen, 1976), and continuous curve 2 is general trend of clinopyroxene evolution in the Grønnedal-Ika intrusion (Halama *et al.*, 2005).

Filling ratios commonly range from 0·80 to 0·95, but are fairly constant within single trails.

Fluid inclusions in hydrothermal fluorite samples of SM1 are typically characterized by a salinity of <5 wt % NaCl eq. Sample JS16 has two types of fluid inclusion, one with high salinity >15 wt % NaCl eq. and another with <10 wt % NaCl eq. Quartz sample JS10 is dominated by secondary fluid inclusions with salinities varying from 6 to 9 wt % NaCl eq. Fluid inclusions in quartz from JS277 were either too small for microthermometry or showed metastable melting. Therefore, a mean salinity of 8·6 wt % NaCl eq. was used for calculating the ion content (see crush–leach results below). In fluorite samples from SM4, fluid inclusions with low salinities <5 wt % NaCl eq. predominate. Higher salinity fluid inclusions (up to 25 wt % NaCl eq.) commonly show brownish ice colours. Hydrothermally formed fluorites from SM5 (JS110, JS175, JS109) show two types of salinities: <5 wt % NaCl eq. and in the range of 7–11 wt % NaCl eq.

Eutectic melting temperatures (T_{me}) generally range from −40 to −28°C. The low T_{me} around −40°C and the

Table 4: Representative microprobe analyses of Fe–Ti oxides

JS:	196	196	196	171	172	172	108	180	180	180	181	164	166
Unit:	SM1	SM1	SM1	SM4	SM4	SM4	SM5	SM5	SM5	SM5	SM5	SM6	SM6
Mineral:	Ilm	Mt	Mt	Mt	Mt	Hm	Mt	Mt	Ilm	Ilm	Mt	Hm	Hm
wt %													
TiO_2	51·10	12·12	1·88	8·01	9·32	0·08	16·00	22·19	51·11	51·23	19·69	0·62	2·80
Al_2O_3	0·02	0·11	0·09	0·18	0·19	0·10	0·13	0·06	0·01	0·00	0·08	0·05	0·36
FeO	40·80	81·41	90·45	84·94	83·61	90·37	76·76	71·85	38·45	41·06	74·37	89·27	86·14
MnO	8·30	2·13	0·37	1·72	1·68	0·06	2·98	3·09	10·68	7·44	2·37	0·36	0·35
MgO	0·00	0·00	0·00	0·02	0·00	0·01	0·00	0·00	0·00	0·00	0·03	0·00	0·00
Total	100·22	95·77	92·79	94·87	94·80	90·62	95·87	97·19	100·25	99·73	96·54	90·30	89·65
Formula based on 2 (3) cations and 3 (4) anions for ilmenite (Ilm) and hematite (Hm) (magnetite, Mt)													
Al	0·00	0·00	0·00	0·01	0·01	0·00	0·01	0·00	0·00	0·00	0·00	0·00	0·01
Ti	0·97	0·35	0·05	0·23	0·27	0·00	0·46	0·63	0·96	0·97	0·56	0·01	0·06
Fe^{3+}	0·07	1·30	1·88	1·53	1·45	1·98	1·08	0·74	0·07	0·05	0·87	1·97	1·84
Mg	0·00	0·00	0·00	0·00	0·00	0·00	0·00	0·00	0·00	0·00	0·00	0·00	0·00
Fe	0·79	1·28	1·04	1·17	1·21	0·01	1·36	1·53	0·74	0·81	1·48	0·01	0·06
Mn	0·18	0·07	0·01	0·06	0·05	0·00	0·10	0·10	0·23	0·16	0·08	0·01	0·01
Sum	2·00	3·00	3·00	3·00	3·00	2·00	3·00	3·00	2·00	2·00	3·00	2·00	2·00

brownish ice colour of the higher salinity fluid inclusions indicate that salts other than NaCl are present in the fluid (e.g. Ca_2Cl, $FeCl_2$, $MgCl_2$, etc., see below; Shepherd *et al.*, 1985; Davis *et al.*, 1989; Borovikov *et al.*, 2001). In addition, trace amounts of CO_2 and CH_4 were detected during isotope analyses.

All fluid inclusions homogenize to the liquid usually between 110 and 230°C. The dominant low-salinity fluid inclusions scatter over the whole temperature range independent of sample or unit. However, the higher salinity fluid inclusions (>10 wt % NaCl eq.) tend to have lower homogenization temperatures and may be interpreted as a later fluid phase present at lower temperatures, but still related to the same magmatic event (as later tectonic, metamorphic or magmatic events in the area are unknown; Upton & Emeleus, 1987).

(1b) *Saline–aqueous three-phase inclusions*. In contrast to the two-phase inclusions described above, three-phase fluid inclusions additionally contain a solid phase (calcite; determined by Raman spectroscopic analyses; Fig. 8c–f). In general, they have a similar shape and size to the two-phase inclusions. The three-phase fluid inclusions occur not only as primary inclusions in nepheline (SM4, SM5), but also along secondary trails in hydrothermal fluorite. In these trails, the phase proportions of calcite–fluid–vapour are fairly constant (Fig. 8). In a few of the 'fluid' inclusions (sample JS109) the calcite minerals are very large and the inclusions contain up to 65 wt % calcite (recalculated using the densities of calcite and fluid). These 'fluid' inclusions may be better referred to as carbonatite melt inclusions. In general, the fluid inclusions containing calcite show a melting behaviour very similar to fluid inclusions of type (1a). However, the calcite predominantly occurs in inclusions with low salinities (Table 7). During heating experiments up to 450°C (at which temperature most inclusions decrepitated), the calcite never dissolved.

(2) *Pure CO_2 fluid inclusions*. Apart from types (1a) and (1b), one fluorite sample (JS34) contain rounded to elongated (<50 μm) fluid inclusions of pure CO_2. These inclusions occur either in groups or within secondary trails together with aqueous fluid inclusions. Their melting temperatures range from −56·8 to −57·9°C and they homogenize to the vapour at temperatures between +28 and +34°C.

(3) *Aqueous–CH_4 fluid inclusions*. Magmatic fluorite from the agpaitic unit SM6 (JS88 and JS122) contains one- or two-phase (CH_4-bearing) fluid inclusions (Fig. 8g and h). They occur either along (pseudo-)secondary trails or (rarely) as isolated groups in which case they may be interpreted to be of primary origin. The fluid inclusions generally have a rounded to irregular shape and are up to 40 μm in size. They range from pure methane with homogenization temperatures between −75 and −93°C to mixed aqueous–methane inclusions. The aqueous–methane proportions vary considerably as methane clathrate does not always form during the heating–freezing experiments. The final ice melting temperatures of the inclusions scatter between −14 and −2°C and are not constant within

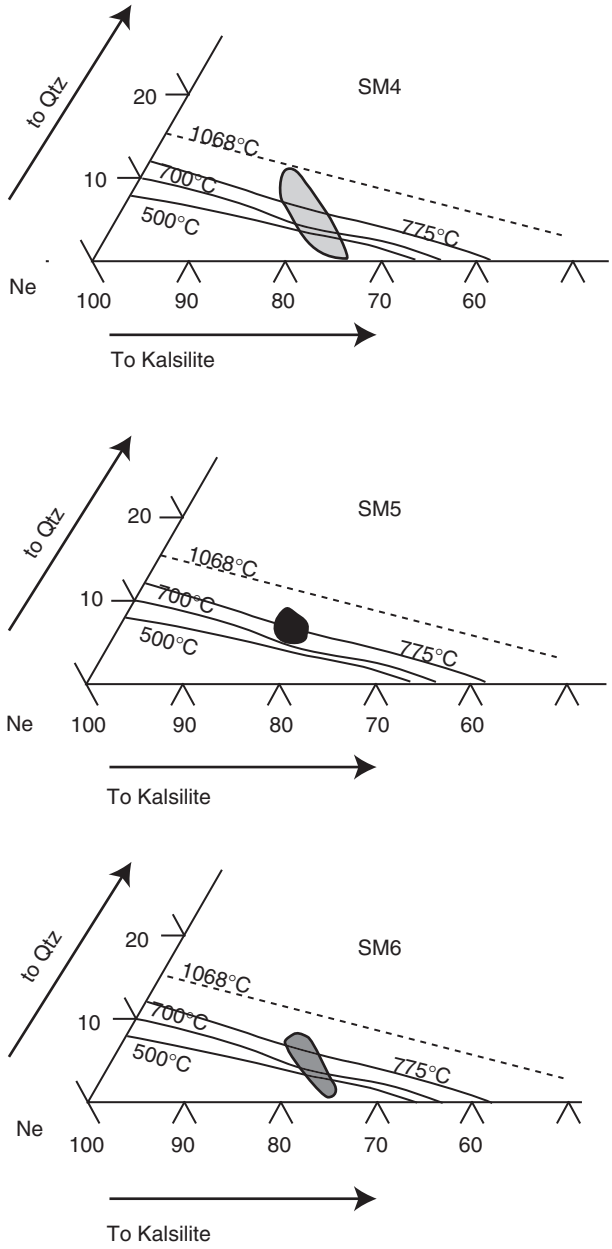

Fig. 5. Composition of nepheline analyzed in this study with isotherms from Hamilton (1961). The compositions are very similar to those reported by Jones (1980).

single trails. Methane clathrate melts between +3 and +21 °C. No higher hydrocarbons or any other components were detected by Raman spectroscopy.

Ion chromatographic analyses

Ion chromatographic analyses of fluid inclusions were performed on fluorites and one quartz sample from SM1, SM4 and SM5. For samples finely intergrown with feldspar, no cation contents are reported, because of contamination effects during the analysis and preparation procedure. The absolute ion concentration was calculated using the average salinity of the sample (Table 8). The calculations were performed using a Cl-factor, which was calculated according to the following equation:

$$\mathrm{Cl} = (\text{atom weight Cl/atom weight NaCl}) \times 10000 \times \text{salinity (wt \% NaCl eq.)}.$$

Chlorine content is up to 10 wt %, and Cl is by far the most abundant anion in the analyzed samples. Nitrate content is below 5000 ppm but is up to 1·1 and 2·0 wt % in samples JS109 and JS152, respectively. The significance of these values and the nitrogen species originally present in the fluid before sample preparation is not clear and we do not suggest that the fluid contained magmatic nitrate. The sulphate concentration is very low (<170 ppm). Bromine content is up to 820 ppm and averages around 400 ppm. The Cl/Br (weight) ratio is between 88 and 124 with two values at 268 and 356 (close to the value for modern seawater).

The dominant cation is Na, with values up to 10·7 wt %. The second most abundant cation is K with values up to 9000 ppm, but usually below 4000 ppm. Mg content ranges from 34 to 4558 ppm, averaging around 900 ppm. Ba content is very low with values <200 ppm; Sr is mostly masked by overlapping Ca but has contents <130 ppm in the two analyzed samples.

The anion–cation charge balance is always >1 because Ca and F were not quantified during the analyses because of their abundance in the host mineral (fluorite). However, a fluorine-free charge balance allows calculation of the minimum amount of Ca in the fluid. This estimation indicates that Ca is the second most abundant cation, with contents ranging from 0·2 to 2·5 wt % and with a mean Na/Ca ratio of 4·5 (except JS6). This is in agreement with the one analyzed quartz sample (JS277, Table 8), which gave an anion–cation ratio of 1·06 and a Na/Ca ratio of 4·0.

Isotopic composition of the fluid inclusions in fluorite

The δD of the inclusion water varies between −40·7 and −135·6‰ (VSMOW, Table 9, Fig. 10). $\delta^{18}O$ values range from −5·7 to −20·9‰ (VSMOW). The $\delta^{13}C$ and $\delta^{18}O$ of inclusion CO_2 ranges from −2·5 to −17·4‰ (VPDB) and from +26·7 to +42·7‰ (VSMOW), respectively (Fig. 7). The $\delta^{13}C$ of inclusion methane could be determined in all samples and ranges from −27·2 to −30·9‰ (VPDB, Fig. 11). The hydrogen isotopic composition of methane could not be determined in all of the samples, as the recovered amount of hydrogen was too small to be analyzed in some cases. However, where analysis was possible, $\delta D_{methane}$ values of −174 to −195‰ (VSMOW) were obtained, which are within the range of values measured in samples from other nepheline syenitic intrusions (e.g. Potter & Konnerup-Madsen, 2003; Graser *et al.*, in press).

Table 5: Nd, O and H isotopic compositions of mineral separates

Sample	Unit	Mineral	Sm (ppm)	Nd (ppm)	$^{147}Sm/^{144}Nd$	$^{143}Nd/^{144}Nd$	$\varepsilon Nd_{(i)}$	T_{DM} (Ga)	$\delta^{18}O$	δD
JS195	SM1	Am	48·52	286·06	0·1026	0·511857 ± 6	0·14	1·77	4·2	−120·1
JS196	SM1	Am	35·29	208·78	0·1022	0·511877 ± 8	0·60	1·74	4·6	−127·6
326012	SM2	Am	84·23	526·96	0·0966	0·511818 ± 9	0·36	1·73	5·3	−132·3
JS171	SM4	Am	20·98	141·91	0·0894	0·511799 ± 9	1·17	1·65	4·8	−111·5
JS172	SM4	Am	31·39	202·50	0·0937	0·511842 ± 7	1·30	1·66	4·7	−109·7
JS108	SM5	Am	14·73	90·50	0·0984	0·511898 ± 10	1·63	1·65	5	−119·1
JS180	SM5	Am	28·28	169·84	0·1007	0·511923 ± 9	1·74	1·65	5	−98·5
JS70	SM6	Px	4·14	19·16	0·1307	0·512131 ± 8	0·90	1·86	5·1	n.a.
JS114	SM6	Px	1·70	12·70	0·0811	0·511793 ± 9	2·40	1·56	4·9	n.a.
JS159	SM6	Px	3·80	18·13	0·1267	0·512123 ± 10	1·40	1·79	4·9	n.a.

ε_{Nd}(i) was corrected to the time of emplacement at about 1·275 Ga (Upton *et al.*, 2003); $\delta^{18}O$ and δD in ‰ (VSMOW). n.a., not analyzed; T_{DM} (Ga), Nd model ages relative to the depleted mantle (Liew & Hofman, 1987).

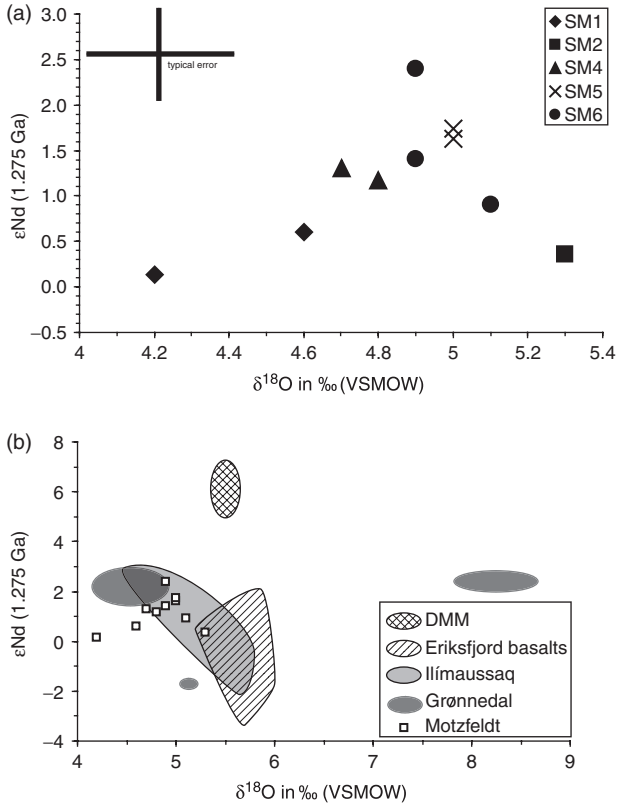

Fig. 6. (a) Initial ε_{Nd} (at $t = 1{\cdot}275$ Ga) vs $\delta^{18}O$ in ‰ (VSMOW) of amphibole (SMl, SM2, SM4, SM5) and pyroxene (SM6) mineral separates. (b) Comparison of data obtained in this study with values from the depleted MORB mantle (DMM; according to DePaolo, 1981; Goldstein *et al.*, 1984; Eiler *et al.*, 2000) and other Gardar rocks (Coulson *et al.*, 2003; Halama *et al.*, 2003, 2005; Marks *et al.*, 2004).

Table 6: $\delta^{13}C$ and $\delta^{18}O$ isotopic composition of Motzfeldt samples (in ‰ VPDB and VSMOW)

Sample	Unit	Type	$\delta^{13}C$	$\delta^{18}O$
JS67	SM4	vein	−4·4	7·8
JS109	SM5	cryst.	−3·9	8·1
JS181	SM5	wr	−3·2	24·2
JS159	SM6	wr	−2·2	21·9
JS164	SM6	wr	−2·1	21·9

vein, calcite vein; cryst, calcite crystals in fluid inclusions; wr, whole-rock samples.

DISCUSSION

Estimation of crystallization temperatures and oxygen fugacity of the Motzfeldt rocks

Both nepheline and feldspar compositions can provide an estimate of the crystallization temperatures of the Motzfeldt rocks. Hamilton (1961; Fig. 5) calibrated the nepheline compositions so that they could be used as a temperature indicator. Based on the maximum values recorded (= crystallization temperatures), the nephelines of the Motzfeldt units SM4, SM5 and SM6 gave temperatures of ~1000°C, ~850°C and ~800°C, respectively, which are in good agreement with the data of Jones (1980) and Jones & Larsen (1985).

Jones (1980) assumed that the feldspars from SM1 to SM5 crystallized at hypersolvus conditions and constrained the minimum temperature of formation of these feldspars to the range 650–800°C. These temperatures are

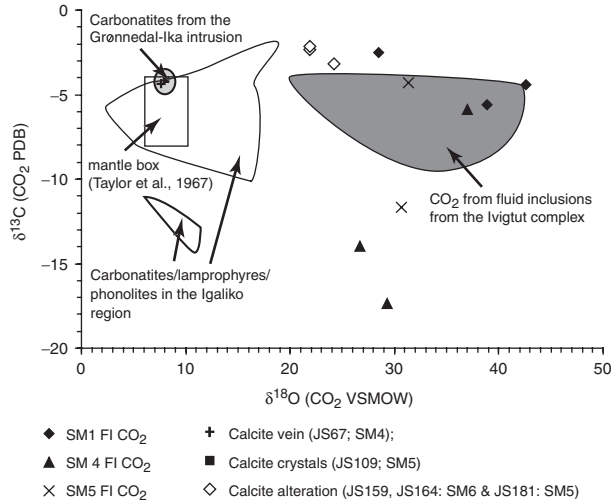

Fig. 7. Isotopic composition of CO_2 from fluid inclusions, calcite from veins, altered samples and calcite crystals from fluid inclusions compared with reference data from other Gardar rocks or fluids (Igaliko region: Pearce & Leng, 1996; Coulson *et al.*, 2003; Ivigtut complex: Köhler *et al.*, 2008; Grønnedal-Ika intrusion: Halama *et al.*, 2005).

slightly lower than the temperature estimates based on nepheline and may reflect solidus rather than liquidus temperatures. The crystallization of two separate feldspars (albite and orthoclase, Fig. 3) in the agpaitic unit SM6 suggests lower crystallization temperatures below the feldspar solvus (e.g. McDowell, 1986; Brown & Parsons, 1989). The very pure endmember compositions indicate temperatures as low as 500°C.

For the miaskitic units, coexisting olivine, clinopyroxene and Fe–Ti oxides can be used to constrain crystallization temperatures, oxygen fugacities and silica activities using two different approaches. Temperature and oxygen fugacities can be obtained for samples containing the coexisting Fe–Ti oxide minerals magnetite and ilmenite provided that they crystallized in equilibrium as assumed for samples JS195–JS197 in SM1 (Fig. 2). Calculations according to Andersen & Lindsley (1985) using the spreadsheet of Lepage (2003) gave temperatures of 640–690°C at f_{O2} values below the FMQ (fayalite–magnetite–quartz) buffer (ΔFMQ −0·8 to −1·3). However, two-oxide thermometry is strictly valid only for quenched (volcanic) rocks, as Fe, Ti and Mg may re-equilibrate at subsolidus conditions. Therefore, the calculated temperatures and oxygen fugacities have to be interpreted with care. However, the results give an approximate indication of the T–f_{O2} conditions that prevailed during the evolution of the Motzfeldt complex.

To at least partially overcome the problem of fast (subsolidus) re-equilibration of the coexisting Fe–Ti oxides, the QUILF approach was used (for the theoretical background, see Frost & Lindsley, 1992; Lindsley & Frost, 1992; Andersen *et al.*, 1993). The QUILF method (software package by Andersen *et al.*, 1993) uses olivine–pyroxene–Fe–Ti oxide equilibria to calculate T–f_{O2} conditions. The temperature is calculated based on Fe, Mg and Ca exchange between clinopyroxene and olivine. Oxygen fugacities and silica activities are calculated using equilibria between Fe–Mg silicates and Fe–Ti oxides. Marks & Markl (2001) gave details of the approach for application to syenitic rocks.

Because of the lack of fresh olivine in our samples (it is rare and altered to iddingsite), we used the olivine and pyroxene compositional data of Jones (1980, 1984). This is justified, as Jones' pyroxene analyses are identical to those in our study (Fig. 4). Hence, we combined his analyses with the Fe–Ti oxide analyses, as these were not analyzed by Jones. Obviously, in doing this, we assume that our Fe–Ti oxide compositions of samples JS181, JS180 and JS108 (from SM5) were in equilibrium with olivine and pyroxene with similar compositions to those reported by Jones (1980, 1984; pyroxene core compositions with high diopside content). With respect to the uncertainty as to whether the minerals really crystallized in equilibrium, the results have to be regarded as rough estimates of T and f_{O2} only. Calculations yielded temperatures from *c.* 600 to 800°C at f_{O2} conditions below the FMQ buffer (ΔFMQ −0·5 to −2) at a_{SiO2} between 0·3 and 0·5. These calculations are in good agreement with the data obtained by two-oxide thermometry and temperature constraints based on nepheline and feldspar compositions. The temperatures have to be regarded as solidus temperatures (e.g. Marks & Markl, 2001). The calculated T–f_{O2} conditions of the miaskitic rocks lie in a region where a CO_2-fluid is stable and only slightly above the CH_4-stability field (Huizenga, 2001, 2005; see discussion below).

Because of the lack of suitable mineral assemblages, the oxygen fugacity for SM6 could not be estimated. However, the high Fe^{3+}/Fe_{total} ratio (Fig. 12, Jones, 1980) and the occurrence of aegirine instead of titanomagnetite and Fe^{2+}-rich amphibole may indicate a higher oxidation state than in the earlier pulses (which does not necessarily mean a higher f_{O2} because of the strong temperature dependence of the f_{O2}–buffer reactions). The late-magmatic alteration to hematite clearly indicates f_{O2} conditions above the hematite–magnetite buffer.

Isotopic constraints derived from mineral separates

The initial ε_{Nd} values (corrected for an age of 1·275 Ga; Upton *et al.*, 2003) are relatively homogeneous, varying by only ±2·3 ε_{Nd} units. The similarity to the Ilímaussaq (Marks *et al.*, 2004) and Grønnedal-Ika intrusions (Halama *et al.*, 2005), the basalts of the Eriksfjord formation (Halama *et al.*, 2003) and Igaliko–Quassiarsuk lamprophyres and carbonatites (Coulson *et al.*, 2003; Fig. 6) suggests that these intrusions or rocks formed from similar mantle sources. The Nd model ages of 1·5–1·8 Ga relative

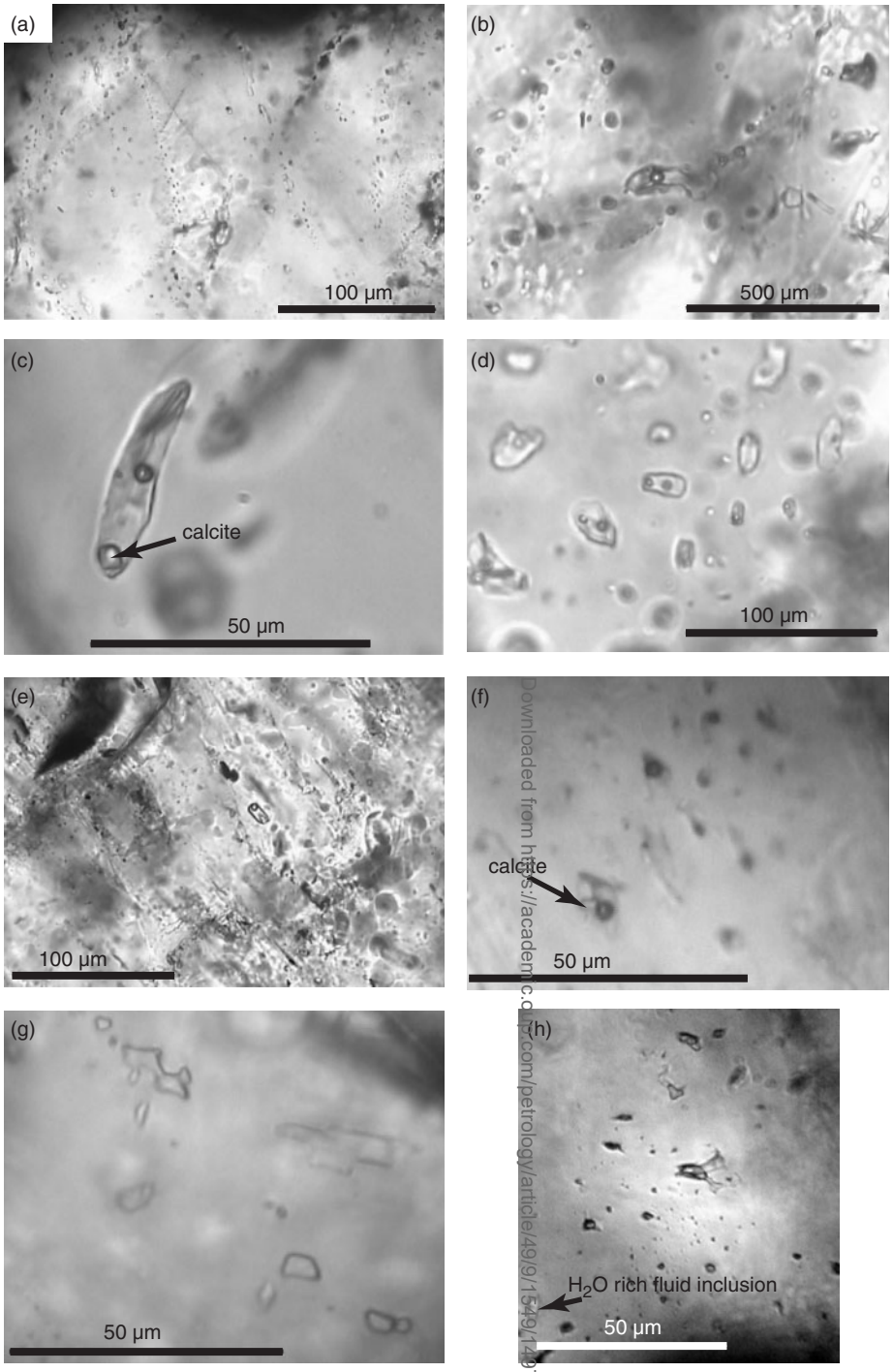

Fig. 8. Typical fluid inclusions (FI). (a) Secondary and pseudo-secondary fluid inclusions [FI type (1a)] from JSl97 (SM1). (b) Secondary fluid inclusions [FI type (1a)] in SM4 (JSl68). (c) Fluid inclusion (FI) with large calcite crystal [FI type (1b)] from SM1 (JSl6). (d) Secondary fluid inclusions with calcite crystals [FI type (1b)] in primary magmatic fluorite from SM1 (JSl97). (e) Primary fluid inclusion (in the centre of photograph) with large calcite crystal [FI type (1b)] in JSl72 (nepheline, SM4). (f) Secondary fluid inclusion with calcite crystals [FI type (1b)] in nepheline (JSl80, SM5). (g) Irregular, pure methane fluid inclusions [FI type (3)] in JS88 (SM6). (h) Irregular, pure methane fluid inclusions [FI type (3)] in JSl22 (SM6; visible bubble because photograph was taken at −110°C) in close association with H_2O-rich fluid inclusion.

Table 7: Microthermometric data for Motzfeldt fluid inclusions

JS	Unit	Mineral	Type	*n*	*T*(me) (°C)	*T*(m) H_2O (°C)	*T*(h) H_2O (°C)	Salinity (wt % NaCl eq.)
6	SM1	fl-sec	(1a) l–v	9	−25 to −48	−1·7 to −14·2	107–284	2·9–18·0
9	SM1	fl-sec	(1a) l–v	7	−28 to −32	−0·6 to −5·8	106–245	1·1–9·0
9	SM1	fl-sec	(1b) l–v–s	2		−2·3 to −7·2		3·9–10·8
10	SM1	qtz-sec	(1a) l–v	34	−20 to −40	−3·8 to −14·1	99–264	6·2–17·9
16	SM1	fl-sec	(1a) l–v	34	−35 to −75	−0·8 to −24·1	111–288	1·4–25·0
16	SM1	fl-sec	(1b) l–v–s	13		−1·0 to −13·2		1·8–17·1
190	SM1	fl-prim	(1a) l–v	14	—	0·0 to −3·1	78–246	0·0–5·1
190	SM1	fl-prim	(1b) l–v–s	5		−0·3 to −1·2		0·5–2·1
197	SM1	fl-prim	(1a) l–v	22	−30 to −40	−0·4 to −6·2	104–362	0·7–9·5
197	SM1	fl-prim	(1b) l–v–s	4		−0·6 to −1·3		1·0–2·2
34	SM4	fl-sec	(1a) l–v	20	−20 to −35	−0·7 to −21·7	94–310	1·2–23·5
34	SM4	fl-sec	(1b) l–v–s	9		−3·1 to −5·0		5·2–7·9
34	SM4	fl-sec	2 CO_2	15		*T*(m) CO_2	*T*(h) CO_2	
						−56·8 to −57·9	28·4–33·5	
90	SM4	fl-sec	(1a) l–v	21	−27 to −38	−1·2 to −6·5	116–256	2·1–9·9
90	SM4	fl-sec	(1b) l–v–s	1		−2·1		3·6
91	SM4	fl-sec	(1a) l–v	7	−30	−0·3 to −4·1	133–328	0·5–6·6
91	SM4	fl-sec	(1b) l–v–s	3		−2·1 to −4·0		3·6–6·5
152	SM4	fl-sec	(1a) l–v	9	−28 to −43	−0·5 to −23·1	119–319	0·9–24·4
152	SM4	fl-sec	(1b) l–v–s	4		−2·1 to −21·5		3·5–23·4
168	SM4	fl-sec	(1a) l–v	10	−30 to −53	−0·5 to −18·6	103–165	0·9–21·4
171	SM4	fsp-prim	(1a) l–v	5	—	−2·7 to −4·7	156–203	4·5– 7·4
172	SM4	ne-prim	(1a) l–v	15	—	−0·7 to −4·3	137–198	1·2–6·9
172	SM4	ne-prim	(1b) l–v–s	9		−0·8 to −2·2		1·4–3·7
225	SM4	fl-sec	(1a) l–v	33	−30 to −50	−0·4 to −24·6	94–193	0·7–25·3
274	SM4	fl-sec	(1a) l–v	10	−28 to −60	−0·5 to −23·1	112–153	0·9–24·4
274	SM4	fl-sec	(1b) l–v–s	1		−3·3		5·5
104	SM5	ne-prim	(1a) l–v	19	-40	−1·9 to −13·1	171–192	3·2 to 17·0
104	SM5	ne-prim	(1b) l–v–s	1		−2·9		4·8
108	SM5	ne-prim	(1a) l–v	10	−25 to −35	−1·7 to −9·8	115–185	2·9–13·7
108	SM5	ne-prim	(1b) l–v–s	2		−3·1 to −3·8		5·1–6·2
109	SM5	fl-sec	(1a) l–v	17	−30 to −47	−0·2 to −7·5	91–216	0·4–11·1
109	SM5	fl-sec	(1b) l–v–s	13		−0·3 to −4·8		0·5–7·6
110	SM5	fl-sec	(1a) l–v	26	−35	−0·4 to −6·9	105–343	0·7–10·4
110	SM5	fl-sec	(1b) l–v–s	4		−0·5 to −2·5		0·9–4·2
175	SM5	fl-sec	(1a) l–v	6	−28 to −29	−0·3 to −3·4	105–163	0·5–5·6
175	SM5	fl-sec	(1b) l–v–s	1		−0·3		0·5
180	SM5	ne-prim	(1a) l—v	22	—	−2·1 to −3·3	136–250	3·5–5·4
180	SM5	ne-prim	(1b) l–v–s	9		−2·7 to −3·2		4·5–5·3
88	SM6	fl-prim	(3) aq. CH_4	5	−40 to −45	−8·0 to −13·9	143–190	11·7–17·7
88	SM6	fl-prim	(3) pure CH_4	3		*T*(m) clathrate	*T*(h) CH_4	
						5·4—13·0	−77·2 to −85·3	
122	SM6	fl-prim	(3) aq. CH_4	17	−35 to −45	−1·9 to −13·8	93–283	3·2–17·6
122	SM6	fl-prim	(3) pure CH_4	17		*T*(m) clathrate	*T*(h) CH_4	
						3·0–21·2	−74·7 to −92·5	

n, number of fluid inclusions analyzed; *T*(me), eutectic melting; *T*(m) H_2O, final melting of ice; *T*(h) H_2O, total homogenization temperature to the liquid. Fluids analyzed in: fl-sec, hydrothermal fluorite; qtz-sec, hydrothermal quartz; fl-prim, primary magmatic fluorite; fsp-prim, primary magmatic feldspar; ne-prim, primary magmatic nepheline. Fluid type: l–v, liquid–vapour two-phase inclusions; l–v–s, liquid–vapour–solid three-phase inclusions; CO_2, pure CO_2-bearing fluid inclusions; aq. CH_4, mixed aqeous–CH_4-bearing inclusions; pure CH_4, pure CH_4 inclusions. *T*(m) clathrate, measured CH_4-clathrate ($CH_4 \times 5{\cdot}75$ H_2O) melting temperatures in mixed aqueous–CH_4-bearing fluid inclusions in JS88 and JS122.

to the depleted mantle (Liew & Hofmann, 1987) are most probably related to the Ketilidian orogeny at this time (Garde *et al.*, 2002) and fall into the range of other model ages for rocks from the Gardar Province (e.g. Marks *et al.*, 2004). Hence, we are dealing with a large magmatic province that is fed from a similar source over a large spatial and temporal interval.

Similar to the Nd isotopic values, the $\delta^{18}O$ values of the minerals define a narrow range (between +4·2 and +5·3‰) and suggest an isotopically rather homogeneous melt throughout the various units. The $\delta^{18}O$ of a nepheline-syenitic melt in equilibrium with the analyzed minerals can be constrained using the approach of Zheng (1993*a*, 1993*b*) and Zhao & Zheng (2003) as shown by Halama *et al.* (2005). Assuming an equilibration temperature of *c.* 800°C, the fractionation between amphibole (hornblende) and melt is −1·6‰, and aegirine–melt fractionation is −0·3‰. Thus the original melt would have a $\delta^{18}O$ between 5·2 and 6·9‰. These values are not only typical mantle values (e.g. Kyser, 1986; Eiler, 2001; Marks *et al.*, 2004), but also $\delta^{18}O$ values characteristic of other syenitic intrusions (e.g. Taylor & Sheppard, 1986; Harris, 1995; Dallai *et al.*, 2003; Marks *et al.*, 2004). The two samples from SM1 show slightly lower $\delta^{18}O$ amphibole values of +4·2 and +4·6‰. Such lower values are usually attributed to interaction with low- $\delta^{18}O$ meteoric fluids (compare O isotopic composition of the fluid inclusions of this study; Marks *et al.*, 2003). The locally intense alteration, the turbidity of feldspars and the occurrence of hydrothermal alteration minerals (e.g. hematite, fluorite, calcite, etc.), especially in unit SM1, support such an interpretation.

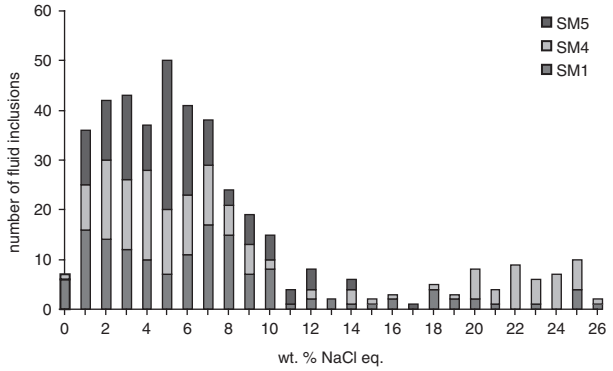

Fig. 9. Histogram of wt % NaCl eq. (calculated after Bodnar, 1993) of all investigated fluid inclusions in the miaskitic units [fluid inclusion types (1a) and (1b)]. (See text for further discussion.)

The δD values are lower than 'normal' magmatic values, which are usually between −50 and −80‰ (see Hoefs, 1997). The most likely process to explain the unusual hydrogen isotopic composition may be post-magmatic interaction with a meteoric fluid, as the hydrogen isotopic composition reacts very easily to the infiltration of an H_2O-rich fluid phase. This is due to its low concentration in minerals compared with oxygen (e.g. Taylor, 1974, 1977). Using the mineral–water fractionation factors for arfvedsonite (at 400°C; Graham *et al.*, 1984) and for hornblende (at 450–800°C; Suzuoki & Epstein, 1976), a coexisting fluid would have a δD of *c.* −60 to −110‰. These values are in good agreement with our isotope analyses of water content of fluid inclusions, which ranges from −40 to −135‰ (δD, VSMOW). If indeed the hydrogen isotopic composition reflects late- to post-magmatic alteration by a meteoric fluid phase, the fluid–rock ratio that caused this shift must have been low, because otherwise it should also be visible in the O isotope compositions.

Table 8: Results of ion chromatography analyses of fluid inclusion content

Sample	Unit	min.	sal.	F^-	Cl^- (a)	Br^-	NO_3^-	SO_4^{2-}	Cl/Br	Na^+	K^+	Li^+	Mg^{2+}	Sr^{2+}	Ba^{2+}	Ca^{2+}	Ca^{2+}†	a/c
JS6	SM1	fl	5·7	n.a.	34472	278	666	49	124	45670	1454	26	80	b.d.	58	n.a.	2096	1·15
JS9	SM1	fl	5·3	n.a.	31751	258	3313	156	123	27839	1998	6	209	b.d.	59	n.a.	7924	1·86
JS16	SM1	fl	11·2	n.a.	67704	190	2884	165	356	56724	3015	38	1115	128	194	n.a.	13350	1·69
JS277	SM1	qtz	8·6*	1353	51897	590	770	65	88	40473	1478	84	1003	57	22	10106	—	1·06
JS152	SM4	fl	14·7	n.a.	88513	489	19832	b.d.	181	107341	4046	18	4558	b.d.	125	n.a.	18803	1·53
JS168	SM4	fl	1·9	n.a.	11497	107	151	5	108	9570	398	1	34	b.d.	b.d.	n.a.	2401	1·80
JS225	SM4	fl	16·3	n.a.	98590	828	635	b.d.	119	67182	3260	13	289	b.d.	45	n.a.	23758	2·12
JS274	SM4	fl	7·9	n.a.	47459	475	3722	31	100	44008	8667	b.d.	1317	b.d.	b.d.	n.a.	6798	1·38
JS109	SM5	fl	5·3	n.a.	31751	311	11029	135	102	n.a.	n.a.	n.a.	n.a.	b.d.	n.a.	n.a.	n.a.	—
JS175	SM5	fl	3·2	n.a.	19469	73	4713	b.d.	268	n.a.	n.a.	n.a.	n.a.	b.d.	n.a.	n.a.	n.a.	—

*Average salinity of all analyzed samples.
†Calculated Ca^{2+} content assuming balanced uncharged fluid, a/c = 1.
All values in ppm except for sal., Cl/Br and a/c ratios. min., host mineral of fluid inclusions; sal., average salinity of fluid inclusions of the sample in wt % NaCl eq.; Cl^- (a), calculated chlorine content; a/c, calculated anion–cation balance (molar), n.a., not analyzed; b.d., below detection limit.

Table 9: Isotopic composition of fluid inclusions (H_2O, CO_2, CH_4)

	Unit	δD_{H2O}	$\delta^{18}O_{H2O}$	$\delta^{18}C_{CH4}$	δD_{CH4}	$\delta^{13}C_{CO2}$	$\delta^{18}O_{CO2}$	$T_{(eq.\ H2O-CO2)}$	$T_{(eq.\ CO2-CH4)}$	$\Delta_{H2O-CO2}$ ($\delta^{18}O$)
JS6	SM1	−95·8	−16·49	−27·21	n.a.	−5·49	38·87	10·0	342·5	55·36
JS9	SM1	−52·4	−9·56	−29·95	−174·1	−2·48	28·50	81·2	260·5	38·06
JS16	SM1	−91·5	−7·55	−28·15	−195·1	−4·46	42·70	26·5	311·0	50·25
JS91	SM4	−135·6	−20·80	−30·85	n.a.	−17·38	29·40	24·0	537·5	50·20
JS225	SM4	−40·7	−5·69	−28·60	−189·9	−5·82	36·87	59·0	325·0	42·56
JS274	SM4	−78·7	−13·96	−29·66	n.a.	−14·03	26·67	66·9	472·5	40·63
JS109	SM5	−76·3	−14·74	−28·18	n.a.	−11·63	30·63	44·5	449·0	45·37
JS175	SM5	−83·2	−12·97	−27·38	n.a.	−4·36	31·34	49·5	321·5	44·32
JS122	SM6	−132·7	−20·86	−29·56	−185·2	n.a.	n.a.			

All values in ‰ VSMOW (for D and O isotopes) and in ‰ VPDB (for C isotopes); $T_{(eq.\ H2O-CO2)}$ and $T_{(eq.\ CO2-CH4)}$ are equilibration temperatures between O and C, respectively (in °C); $\Delta_{H2O-CO2}$ is fractionation water–CO_2 ($\delta^{18}O$).

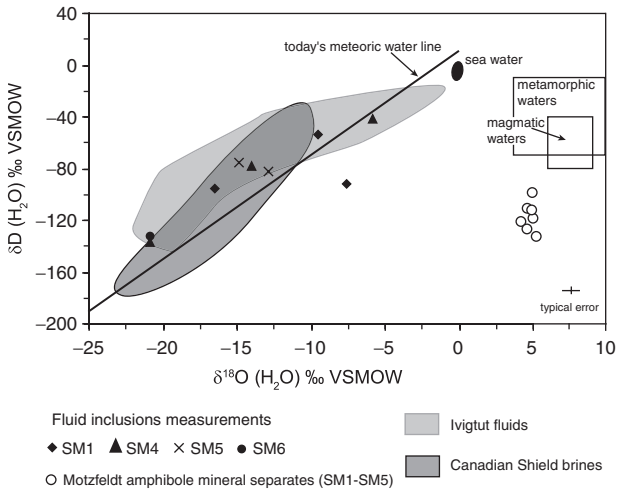

Fig. 10. Isotopic composition of fluid inclusion water. The good agreement with data from the Ivigtut complex fluids (Köhler *et al.* 2008) and Canadian Shield brines (Frape & Fritz, 1982; Frape *et al.*, 1984; Bottomley *et al.*, 1994) should be noted. Reference data for magmatic, metamorphic and meteoric waters from Sheppard (1986).

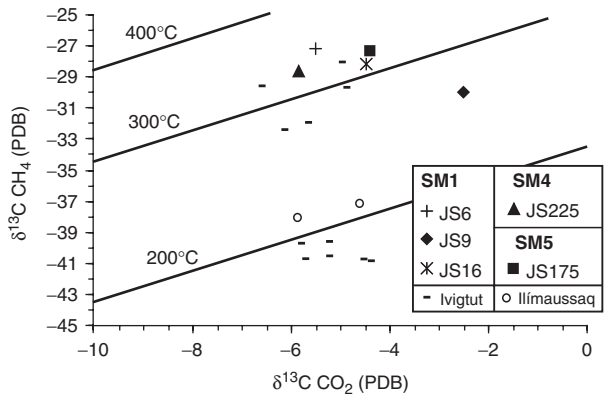

Fig. 11. $\delta^{13}C$ (CH_4) vs $\delta^{13}C$ (CO_2). Equilibration temperatures according to Richet *et al.* (1977). Reference data for Ivigtut and Ilímaussaq from Köhler *et al.* (2008) and Graser *et al.* (in press), respectively.

Other processes that could also cause depleted δD values include extreme degassing of magmatic fluids, assimilation of organic-rich sediments and oxidation of magmatic methane (see Marks *et al.*, 2004). However, no signs of extreme degassing of magmatic fluids, such as the presence of a large contact aureole around the intrusion, are observed and no organic-rich sediments have been described anywhere in the vicinity of the Motzfeldt intrusion or in the Gardar Province as a whole (Marks *et al.*, 2004). Our fluid inclusion study suggests that CO_2 and not CH_4 was the dominant carbon species in the fluid during most of the differentiation history of the Motzfeldt magmas (see below).

The isotopic composition of the calcite from a calcite–fluorite vein lies within the mantle box of Taylor *et al.* (1967; see also Kyser *et al.*, 1982; Des Marais & Moore, 1984; Deines, 1989; Clarke *et al.*, 1993; Keller & Hoefs, 1995; $\delta^{18}O$ 7·8‰; $\delta^{13}C$ −4·4‰). The values are in accordance with analyses by Pearce & Leng (1996), Pearce *et al.* (1997), Goodenough (1997), Coulson *et al.* (2003), Taubald *et al.* (2004) and Halama *et al.* (2005) from various carbonate or carbonatite localities in the Gardar Province, suggesting a common mantle source of the carbonates.

Three whole-rock powders (JS159 and JS164 from SM6; JS181 from SM5) containing considerable amounts of calcite veinlets and/or calcite as an alteration product of feldspar and eudialyte (e.g. Fig. 3) were also analyzed for their C and O isotopic composition. The $\delta^{18}O$ values range from +21·9 to +24·2‰ and $\delta^{13}C$ from −2·1 to −3·2‰ (Fig. 7). Similar values

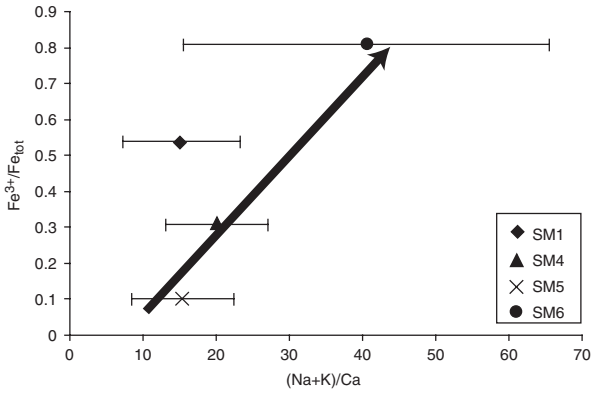

Fig. 12. Fe^{3+}/Fe_{total} vs (Na + K)/Ca for whole-rock data from Jones (1980). The increase in (Na + K)/Ca equals a fractionation increase. As shown by several workers, the arrow may indicate a temperature decrease [= increase in Fe^{3+} and (Na + K)]. The high whole-rock Fe^{3+} content of SM1 is related to the formation of secondary Fe^{3+}-rich minerals. (See text for further discussion.)

for samples from SM1 and SM4 were obtained by J. McCreath (personal communication, 2007). The results are comparable with those obtained by Pearce & Leng (1996) and Coulson *et al.* (2003) from the area around the Motzfeldt intrusion (i.e. Igaliko region). The $\delta^{13}C$ values lie near those reported for mantle rocks (Taylor *et al.*, 1967; Keller & Hoefs, 1995) and therefore possibly suggest mantle derivation. The oxygen isotope values are considerably enriched in ^{18}O with regard to mantle rocks and are more typical of secondary and/or low-temperature alteration of calcite (Deines, 1989; Demény *et al.*, 1998). The slight enrichment of $\delta^{13}C$ and variably enriched $\delta^{18}O$ might be explained by the model of Deines (1989), who stated that $\delta^{18}O$ increases with fractionation and with a decreasing carbonate:silicate ratio (see also Worley *et al.*, 1995). Furthermore, Tichomirowa *et al.* (2006) assumed that increasing $\delta^{18}O$ values could be explained by interaction with water-rich fluids, which is the most likely explanation for the observed heavy oxygen isotopic composition (see below). Hence, only the C isotope signature would probably preserve the mantle record during hydrous alteration if the C concentration of the infiltrating fluid is low. Köhler *et al.* (2008) used a similar explanation for the observed change in $\delta^{18}O$ at constant $\delta^{13}C$ of CO_2 for fluid inclusions from another Gardar intrusion, the Ivigtut complex (see discussion of fluid inclusion results).

Discussion of fluid inclusion results

The fluid inclusions present in primary minerals of the miaskitic units SM1, SM4 and SM5 are of both primary and secondary origin. Their salinities are commonly <6 wt % NaCl eq. The few higher salinity fluid inclusions possibly represent a different (low-temperature) fluid generation.

Regarding the commonly observed calcite crystals in the low-salinity fluid inclusions, we may ask whether these minerals are 'true' daughter minerals or if they are just accidentally trapped solid crystals. The fact that in certain secondary fluid inclusion trails, each fluid inclusion contains a calcite crystal in constant phase proportions (Fig. 8) suggests that these are indeed daughter minerals. They crystallized after entrapment from a fluid originally undersaturated in calcite. However, accidental trapping cannot be completely ruled out for samples in which only few inclusions contain calcite.

The fact that both two-phase (liquid–vapour) and three-phase (liquid–vapour–solid) fluid inclusions occur in the miaskitic rocks provides evidence that during their evolution the fluid was characterized by H_2O and NaCl with variable amounts of CO_2 (or HCO_3^-). Unfortunately, the sample material did not allow us to decipher the exact relative chronologies of entrapment of the two types of fluid inclusions, because of the lack of adequate cross-cutting relationships.

In contrast to the H_2O–NaCl–CO_2 fluid in the miaskitic rocks, fluid inclusions in magmatic fluorite from the agpaitic rocks (SM6) are characterized by H_2O–NaCl–CH_4 without any calcite. The close association of pure methane, mixed H_2O–NaCl–CH_4 and (almost) pure H_2O–NaCl inclusions suggests that they formed from a heterogeneous, but definitely reduced fluid displaying immiscibility.

Based on stratigraphic reconstructions, pressure conditions during emplacement of the Motzfeldt intrusion were probably between 1 and 2 kbar as suggested by Jones (1980). Similar conditions were obtained for the Ilímaussaq intrusion (Konnerup-Madsen & Rose-Hansen, 1984). Accordingly, a pressure correction of 50–100°C has to be applied to the homogenization temperatures of the fluid inclusions. The homogenization temperatures range from 78 to 343°C (Table 7) with the majority lying between 100 and 200°C. Accordingly, formation temperatures between 150 and 300°C can be assumed (Bakker, 2003; not applicable to fluid inclusions from SM6 as they are assumed to be trapped from a heterogeneous fluid). No isochores could be calculated for inclusions containing calcite, as no total homogenization temperature could be determined. Not even partial dissolution of the calcite crystals was observed and it is unclear to us whether the dissolution of the crystals was inhibited kinetically or because the formation temperatures were much higher than the decrepitating ones.

The results of our crush–leach analyses support our microthermometric results indicating that the fluid is, in addition to H_2O, dominated by Na, Cl and minor amounts of Ca. Other ions are only of minor importance. The Cl/Br ratios (by weight) of our samples mostly lie between 95 and 120. The high Cl/Br ratio in sample JS16 may be attributed either to a mixture of a high- and a low-salinity fluid and/or to another fluid generation (higher proportion of higher salinity fluid inclusions in this sample). The predominant low Cl/Br ratios are comparable with those of

other peralkaline Gardar intrusions (Köhler *et al.*, 2008; Graser *et al.*, in press). This similarity across the Gardar Province may suggest a common halogen source, which is in agreement with the Nd isotope-based assumption of a common mantle source of the magmas in general and a common evolution process of the fluid phase. The Cl/Br values of about 100 suggest that unmixing or exsolution of a fluid phase preferentially partitions Br into the fluid relative to the melt and early crystallizing minerals, as suggested by the experiments of Bureau *et al.* (2000) and Bureau & Métrich (2003).

Isotopic composition of inclusion H_2O

In terms of H and O isotopic composition, the water within the inclusions closely follows the present-day meteoric water line (MWL, Craig, 1961) and falls within the published data array for the Ivigtut complex (Köhler *et al.*, 2008) and Canadian Shield brines (Fig. 10; Frape & Fritz, 1982; Frape *et al.*, 1984; Bottomley *et al.*, 1994). However, the isotopic composition of the inclusion water is slightly shifted to the left of the MWL. This may be attributed either to equilibration with CO_2 (Richet *et al.*, 1977; Cartwright *et al.*, 2000; Köhler *et al.*, 2008) or to low-temperature isotopic equilibration with the host-rocks at low water/rock ratios (Frape & Fritz, 1982; Kelly *et al.*, 1986; Sheppard, 1989). A mixing process with a fluid of unknown origin cannot explain the displacement of the data to the left of the MWL as all known 'reservoirs' lie to the right of the MWL (e.g. magmatic or metamorphic waters, Hoefs, 1997). We prefer the second explanation, as the volume of CO_2 in the fluid inclusions is negligible compared with the dominant water–salt mixture (up to 95 mol %). Furthermore, the available fractionation factors between amphibole and water (Suzuoki & Epstein, 1976; Graham *et al.*, 1984) suggest that the hydrogen isotope composition of the inclusion water (δD −40 to −100‰) could represent equilibrium values. The low oxygen isotope values ($\delta^{18}O$ −5 to −25‰) of the inclusion water, however, are not in equilibrium with the analyzed oxygen isotope compositions of the mineral separates ($\delta^{18}O$ +4·2 to +5·3‰). This again points to interaction of a low proportion of meteoric water with the rocks (low fluid–rock ratio; see above, discussion of isotopic composition of mineral separates).

Isotopic composition of inclusion CO_2

In all analyzed samples (except for JS122, SM6), trace amounts of CO_2 were detected during the isotope analyses. The $\delta^{13}C$ values of the CO_2 define two groups (Fig. 7), which may be explained in the following way. $\delta^{13}C$ values between −2 and −6‰ (VDPB) resemble primary magmatic and/or mantle values (Taylor *et al.*, 1967; Keller & Hoefs, 1995). The second group is defined by lower $\delta^{13}C$ values ranging from −10 to −17‰. These lower values are commonly explained by contamination with organic-rich material, which is, however, unknown in the Gardar Province (e.g. Marks *et al.*, 2004). Calcite crystals in the fluid inclusions were observed in (almost) all studied samples irrespective of carbon isotopic composition. Therefore, there seems to be no influence from these crystals on the isotopic composition. However, the fluorite samples with low $\delta^{13}C$ values are very finely intergrown with carbonates. The fractionation of carbon between calcite and CO_2(aq) based on the fractionation factors of Ohmoto & Goldhaber (1997) is 8‰ at low temperatures (20–50°C). Such a fractionation could account for the difference in carbon isotopes between the two groups (even regarding the fact that calcite intergrowths were removed by treating the samples with acid prior to analysis). However, the geological significance of this process remains enigmatic.

The very similar range of $\delta^{13}C$ values of −4 to −14·1‰ obtained for lamprophyres, phonolites and carbonatites from the Motzfeldt (Igaliko) region (Fig. 7; Pearce & Leng, 1996) points to a common carbon isotopic source and evolution in the whole region and in different rock types, inviting speculation about CO_2 metasomatism in the mantle source region.

The $\delta^{18}O$ value of inclusion CO_2 ranges from +26·7 to +42·7‰ (VSMOW). The inclusion CO_2 is considerably enriched in ^{18}O and is much higher than normal carbonatitic mantle values (Fig. 7; e.g. Taylor *et al.*, 1967; Halama *et al.*, 2005). We follow the argumentation of Köhler *et al.* (2008), who pointed out the similarity in isotopic composition to CO_2 vesicles in mid-ocean ridge basalt (MORB) (Pineau & Javoy, 1983). They explained these high values by low-temperature isotopic exchange with oxygen from the inclusion water. Using the fractionation factors of Friedman & O'Neill (1977), the fractionation of oxygen between CO_2 and H_2O(aq) is around 40‰ at low temperatures (10–100°C). This is in accordance with the work of Richet *et al.* (1977), who reported a fractionation of 41·2 to 44·1‰, which may even be increased by the presence of dissolved salts in the fluid inclusions (Pineau & Javoy, 1983). The fractionation for the samples from the Motzfeldt intrusion ranges between 38·1 and 55·4‰, with a mean of 46·3‰, comparable with the data of Richet *et al.* (1977) and Köhler *et al.* (2008).

Isotopic composition of inclusion CH_4

The carbon isotopic composition of CH_4 in the inclusions is fairly constant ($\delta^{13}C$ −27 to −31‰ VPDB). Even the isotopic composition of CH_4 from fluorite in the agpaitic unit is within the range of the samples from the miaskitic rocks. Calculating the C isotopic equilibration temperatures between methane and CO_2 using the fractionation factors of Richet *et al.* (1977) results in values of 300–350°C (only $\delta^{13}C$ values of CO_2 from samples in which the CO_2 has a mantle-like carbon isotopic composition were used; see above). These temperatures are only slightly higher than those deduced from the pressure-corrected fluid inclusion temperatures.

As no sign of organic material is found within the Gardar Province, the low $\delta^{13}C$ values of CH_4 in the

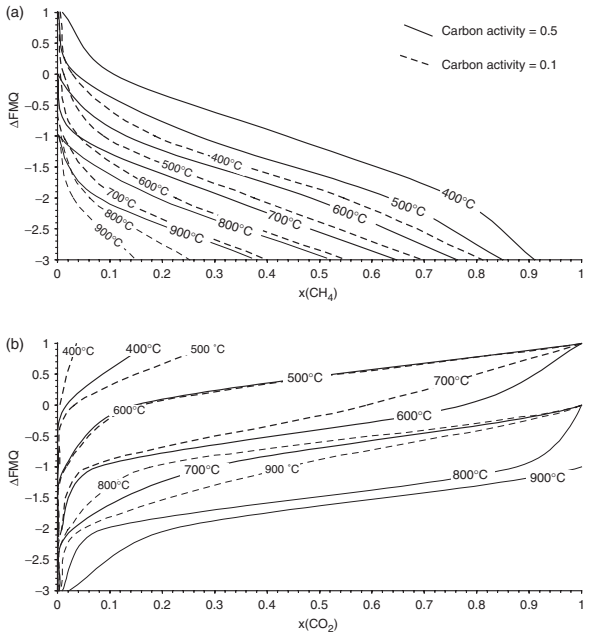

Fig. 13. (a) $x(CH_4)/[x(CH_4)+x(CO_2)+x(H_2O)]$ vs oxygen fugacity in the relevant T–f_{O2} range (oxygen fugacity given as ΔFMQ). Different modelled curves represent $x(CH_4)$ in the fluid for different temperatures and carbon activities at 1 kbar calculated according to Huizenga (2001, 2005). At a constant relative oxygen fugacity (i.e. constant ΔFMQ), the $x(CH_4)$ increases with decreasing temperature. (b) Same as (a) but with $x(CO_2)/[x(CH_4)+x(CO_2)+x(H_2O)]$ vs oxygen fugacity given as ΔQFM. At constant relative oxygen fugacity (i.e. constant ΔFMQ), the $s(CO_2)$ in the fluid decreases with decreasing temperature.

inclusion cannot be attributed to a thermogenic origin related to the thermal decomposition of organic material (Schoell, 1988). However, Konnerup-Madsen *et al.* (1985), Kogarko *et al.* (1987) and Ryabchikov & Kogarko (2006) have suggested that the formation of methane may be explained by the respeciation of an originally CO_2–H_2O-rich fluid upon temperature decrease (see Figs 13 and 14). Given the calculated equilibration temperatures, this mechanism appears plausible also for our samples.

The transition from miaskitic to agpaitic rocks

The transition from the miaskitic units SM1–SM5 to the agpaitic SM6 can be observed in the change in mineralogy, fluid composition, whole-rock alkali content and Fe^{3+}/Fe^{2+}. These changes should be related to a common process.

Mineralogical change

The change from miaskitic to agpaitic mineral assemblages (zircon and titanite to eudialyte) and from (Fe^{2+}-rich) amphibole- to (Fe^{3+}-rich) aegirine-dominated mafic minerals in very late-stage magmatic rocks may be related to several partly interrelated causes, as follows.

(1) Change in oxidation state: a dominance of Fe^{3+} over Fe^{2+} in the melt would effectively inhibit the crystallization of amphibole, which commonly has a rather low Fe^{3+} content ($Fe^{3+}/Fe^{2+}<0{\cdot}4$ in Ilímaussaq, Marks *et al.*, 2007; see also Leake, 1997). Crystallization of aegirine would be a direct consequence of a change in oxidation state.

(2) A change of the melt's alkali (Na)/iron ratio: arfvedsonite has an alkali (Na)/Fe ratio of 0·6, whereas aegirine has a ratio of 1; increasing alkalis relative to iron could drive a melt towards aegirine crystallization irrespective of redox conditions. Although nominally unrelated to redox conditions, crystallization of Fe–Ti oxides would effectively increase this ratio. Their crystallization, however, is again highly redox-dependent.

(3) The formation of a water-deficient fluid resulting from the methane-producing reaction

$$CO_2 + 2\ H_2O = CH_4 + 2\ O_2. \qquad (1)$$

Apart from consuming water and possibly inhibiting the formation of 'water-rich' amphibole, this reaction could be responsible for an increase of 'free' oxygen, which in turn could further oxidize the iron in the melt.

(4) The formation of eudialyte may be mainly related to the increased solubility of Zr (and possibly other HFSE; e.g. Kogarko, 1974; Watson, 1979; Watson & Harrison, 1983; Farges *et al.*, 1991; Hanchar & Watson, 2003) in peralkaline melts because a high alkali/Al ratio inhibits crystallization of zircon or baddeleyite (Nicholls & Carmichael, 1969; Hoskin & Schaltegger, 2003). Finally and very importantly, the early exsolution of a hydrous fluid phase is inhibited as a result of the high alkalinity and low water activity. This retains Na, halogens and consequently also Zr and other HFSE in the melt (Kogarko, 1974; Treuil *et al.*, 1979; Taylor *et al.*, 1981). Therefore, the formation of eudialyte can be assumed to be a consequence of the high concentration of alkalis, the long crystallization interval and the inhibited exsolution of a fluid phase associated with the reduced conditions.

Change in fluid composition

The change in fluid composition from an H_2O–HCO_3–NaCl–$CaCl_2$ to a CH_4–H_2O–NaCl–$CaCl_2$(?) fluid can be explained by combining the T–f_{O2} data detailed above with theoretical calculations by Huizenga (2001, 2005), who used fugacity coefficients from Shi & Saxena (1992). Figure 13 shows that a CO_2–H_2O-dominated fluid at high temperatures generally evolves to a fluid dominated by CH_4–H_2O at lower temperatures at constant relative oxygen fugacities (expressed as ΔQFM in Fig. 13; see Konnerup-Madsen, 2001; Ryabchikov & Kogarko, 2006; Fig. 14) if f_{O2} is buffered by a mineral assemblage such as olivine–spinel–clinopyroxene–feldspar, in which clinopyroxene and feldspar buffer a_{SiO2} because of Ca-tschermakite- or jadeite-involving equilibria. This is in accordance with calculations using thermodynamic data from Robie & Hemingway (1995) assuming ideal gas behaviour, a C : H ratio of 0·5 and a pressure of

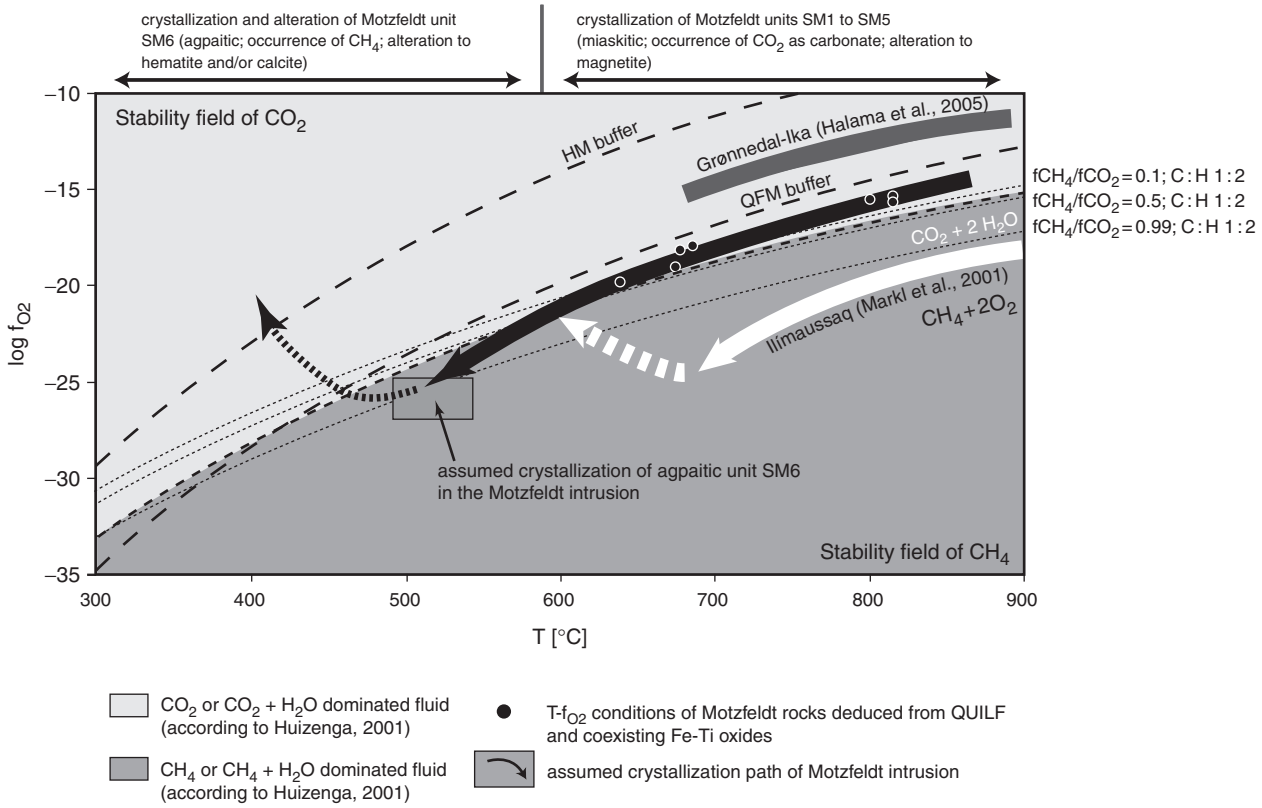

Fig. 14. Assumed crystallization path of the Motzfeldt intrusion (bold black line). The miaskitic rocks formed at high temperatures within the stability field of CO_2 [calculated according to Huizenga (2001) and using the thermodynamic data of Robie & Hemingway (1996)]; the fine dotted lines represent varying CH_4/CO_2 fugacities. In the course of crystallization and as a result of a temperature decrease, the Motzfeldt magma entered the stability field of CH_4 which led to the crystallization of the agpaitic unit SM6. The final increase in oxygen fugacity is evidenced by post-magmatic hematite and/or calcite. Compared with other Gardar intrusions, the Motzfeldt intrusion has an intermediate position between the oxidized and CO_2-(calcite)-dominated miaskitic Grønnedal-Ika intrusion (dark grey line: Halama *et al.*, 2005) and the CH_4-dominated reduced agpaitic Ilímaussaq complex (white line: Markl *et al.*, 2001).

1 kbar with variable $f(CH_4)/f(CO_2)$ ratios (Halama *et al.*, 2005; Fig. 14). Additionally, the H/O ratio of the fluid may also be important for equilibrium (1), as a high H/O ratio favours hydrocarbons and a low H/O ratio favours carbon dioxide (e.g. Huizenga, 2001, 2005). Figure 14 shows that the calculated T–f_{O2} conditions for the miaskitic rocks from the Motzfeldt intrusion lie within the CO_2–H_2O stability field, just slightly above the transition curve relating a CO_2–H_2O with a CH_4–H_2O fluid. The evolution to lower temperatures at a constant relative oxygen fugacity may explain the observed change of the composition to a CH_4–H_2O-dominated fluid in the agpaitic rocks. Obviously, only a slight decrease in oxygen fugacity caused by, for example, the increase in the melt's alkali content, may also influence the carbon speciation in the fluid (see discussion below).

Fischer-Tropsch (F-T) type reactions (e.g. Salvi & Williams-Jones, 1997, 2006) are not believed to be important, as no sign of higher hydrocarbons and/or H_2 was found in the fluid inclusions, nor are the CH_4-bearing fluid inclusions associated with the breakdown of hydrous minerals which would be necessary to trigger F-T-type reactions (e.g. Nivin *et al.*, 2005; Salvi & Williams-Jones, 2006). A mixing process involving meteoric and magmatic water, which may be important for the formation of methane as suggested by Potter *et al.* (1999) and Nivin *et al.* (2005), is questionable for the Motzfeldt intrusion as no CH_4-bearing fluid inclusions were found in samples from the miaskitic rocks. The trace amounts of methane found during isotope analyses in the fluid inclusions may be more easily explained by the proposed respeciation model (Konnerup-Madsen *et al.*, 1985; Ryabchikov & Kogarko, 2006).

The change in mineralogy (from Fe^{2+}- to Fe^{3+}-bearing mafic minerals) is closely linked to the change in fluid composition (from CO_2 to CH_4), but it is very important to note that these changes work in different directions: whereas the first requires oxidation, the second requires reduction.

The whole-rock compositional change from Fe^{2+}- to Fe^{3+}-dominated linked to alkali content and C–O–H speciation

Generally, the speciation of a C–O–H fluid as well as the oxidation state of Fe is closely linked to the oxidation state

of the magma (Bezos & Humler, 2005). Assuming fractional crystallization in a system closed with respect to oxygen (Byers *et al.*, 1984), the Fe^{3+}/Fe_{total} ratio commonly increases (Bezos & Humler, 2005). As it is difficult to envisage how a magmatic system can be closed to oxygen diffusion, Bezos & Humler (2005) suggested that the Fe^{3+}/Fe^{2+} ratio of a basaltic melt increases as a result of the highly compatible behaviour of Fe^{2+} in olivine and the strong incompatibility of Fe^{3+} in olivine and plagioclase. Although we are obviously not dealing with an olivine-fractionating system, the preferred uptake of Fe^{2+} by, for example, amphibole, ulvöspinel-rich titanomagnetite or ilmenite would explain the increasing Fe^{3+}/Fe^{2+} in the Motzfeldt melt.

In magmatic systems, ferric and ferrous iron are related by the following equilibrium (e.g. Rüssel & Wiedenroth, 2004):

$$4\ Fe^{3+} + 2\ O^{2-} \leftrightarrow 4\ Fe^{2+} + O_2. \quad (2)$$

It has been shown by a number of workers (Kress & Carmichael, 1988; Lange & Carmichael, 1989; Gerlach *et al.*, 1998, 1999; Rüssel & Wiedenroth, 2004) that equilibrium (2) is shifted to the left with decreasing temperature and increasing Na and K content of the melt (e.g. Kress & Carmichael, 1991; Rüssel & Wiedenroth, 2004), which fits with the observations at Motzfeldt (Fig. 12; Jones, 1980). Accordingly, the peralkalinity of a melt and the degree of oxidation of iron (i.e. the stability of Fe^{2+} vs Fe^{3+}) are strongly related (Sack *et al.*, 1981; Kilinic *et al.*, 1983; Kress & Carmichael, 1989, 1991; Lange & Carmichael, 1989; Gerlach *et al.*, 1999; Rüssel & Wiedenroth, 2004). Using the empirical equation of Kress & Carmichael (1991) to calculate the oxygen fugacity in silicate liquids, an increase in the peralkalinity index [molar (Na + K)/Al] from 0·9 to 1·3 can lead to a decrease in oxygen fugacity by 0·5 $\log f_{O2}$ units (at constant Fe^{2+}/Fe^{3+} ratio). Furthermore, there is the petrographic observation that agpaitic mineral assemblages are confined to very highly differentiated, extremely alkaline rocks (e.g. Khomyakov, 1995; Sørensen, 1997; Markl *et al.*, 2001), which commonly have a high Fe^{3+}/Fe^{2+} ratio.

A related reaction can be easily derived by combining reactions (1) and (2):

$$8\ FeO^{melt} + CO_2 + 2\ H_2O \leftrightarrow CH_4 + 4Fe_2O_3^{melt}. \quad (3)$$

This reaction describes the magmatic evolution of the Motzfeldt intrusion in a simple way. It takes into account the observed change from an Fe^{2+}-dominated miaskitic mineral assemblage in Motzfeldt units SM1–SM5 to the Fe^{3+}-dominated agpaitic rocks of SM6. Furthermore, it also includes the observed transition in the fluid phase from (H_2O–NaCl)–CO_2 in the miaskitic rocks to (H_2O–NaCl)–CH_4 in the agpaitic rocks.

Late-stage alteration phenomena involving peralkaline fluids

In general, late- to post-magmatic metasomatism involving a Na-rich fluid at higher relative oxidation state is typical of peralkaline magmatic complexes (Salvi & Williams-Jones, 1990; Nivin *et al.*, 2001, 2002, 2005; Marks *et al.*, 2003, 2004; Potter *et al.*, 2004; Halama *et al.*, 2005; Beeskow *et al.*, 2006; Schönenberger *et al.*, 2006; Fig. 14). For Motzfeldt, Jones & Larsen (1985) suggested that there was a continuous evolution from a low-*T*, peralkaline, volatile-rich melt that formed the agpaitic rocks (SM6) to a hydrothermal solution containing excess sodium (e.g. Tuttle & Bowen, 1958; Khomyakov, 1995). This fluid would be an efficient agent for metasomatism, especially in the roof zone of the intrusion (Jones & Larsen, 1985). The action of such a fluid is evidenced, especially in SM1, by the presence of secondary aegirine–augite or aegirine and the common occurrence of late-stage calcite or cancrinite, which records a Na- and HCO_3-bearing fluid. Jones & Larsen (1985) assumed that these alteration fluids had trace element characteristics similar to those of the lujavritic melts and therefore enriched the altered syenites with some trace elements up to sub-economic values.

In the agpaitic rocks, fluid metasomatism led to destabilization of the agpaitic assemblage (eudialyte, aegirine, CH_4) and sodalite was replaced by analcime and nepheline by sodalite + analcime, comparable with the reactions described by Markl *et al.* (2001) for the Ilímaussaq intrusion. The alteration of eudialyte resembles the textures described from the nearby North Qoroq intrusion (Coulson, 1997), stabilizing miaskitic minerals such as zircon, allanite-(Ce), natrolite, hematite and calcite (Fig. 3). Mitchell & Liferovich (2006) suggested that this alteration of a primary magmatic agpaitic to a miaskitic assemblage may be explained by changing pH (see Khomyakov, 1995; Markl & Baumgartner, 2002).

SUMMARY AND CONCLUSIONS

Magmatic and fluid evolution of the Motzfeldt intrusion

The chemical evolution of the various magmatic units of the Motzfeldt intrusion suggests one continuous crystallization sequence. Fe^{2+}-rich miaskitic mineral assemblages are followed by a late-stage Fe^{3+}-rich agpaitic mineral assemblage. Based on the Nd and O isotopic composition of mineral separates, both the miaskitic and the agpaitic rocks in the Motzfeldt intrusion appear to have been derived from the same magma source and show minimal signs of crustal contamination. Hence, their different mineralogical and geochemical evolution must be explained in terms of fluid–melt partitioning and/or magmatic differentiation processes. The Motzfeldt rocks formed at oxygen fugacities below the

FMQ buffer; however, the presence of late-stage alteration products such as hematite suggests higher oxygen fugacities above the HM (hematite–magnetite) buffer during the waning stages of magmatism.

Studies of fluid inclusions in fluorite, nepheline and quartz have revealed the presence of a Na- and Cl-dominated fluid with a salinity of <10 wt % NaCl eq. All the miaskitic units show evidence of oxidized fluid compositions and the presence of calcite points to considerable amounts of HCO_3^- in the system. In contrast, the agpaitic unit SM6 contains reduced H_2O–NaCl–CH_4 fluid inclusions. It is interesting to note that the T–f_{O2} conditions derived for the miaskitic units only barely lie in the field of CO_2 dominance in the fluid (Fig. 14). Accordingly, a small change in any parameter related to f_{O2} can push the fluid and thereby the whole system into the CH_4 stability field, and may thereby cause agpaitic assemblages to form. The similar fluid isotopic composition of the miaskitic and agpaitic rocks indicates that not only the minerals or rocks but also all the Motzfeldt fluids were derived from a similar source. Combining the carbon isotopic composition, which partially reflects a mantle origin, with the hydrogen and oxygen isotope compositions of the inclusion water, which imply a meteoric origin, a fluid mixing model best explains the fluid assemblage observed in the Motzfeldt rocks. This seems to be similar to the case of the South Greenland Ivigtut complex (Köhler *et al.*, 2008) and at least the late-stage hydrothermal fluids in the Ilímaussaq intrusion (Graser *et al.*, in press).

We suggest that the association of a reduced mineral assemblage (Fe^{2+}-dominated minerals) and an oxidized fluid (CO_2, calcite) progressively changes during magmatic differentiation to an oxidized mineral assemblage (Fe^{3+}-bearing; aegirine) and a reduced fluid (CH_4) in the last crystallizing rock unit (SM6). These changes are probably mainly driven by respeciation during temperature decrease and the increasing alkali content of the melt. The lujavrites in the Motzfeldt intrusion formed from these very highly fractionated, late-stage melts.

Comparison with other intrusions

On the basis of Nd and O isotope data, the source of the Motzfeldt magmas seems to be similar to that of the other Gardar intrusions (Ilímaussaq: Marks *et al.*, 2004; Puklen: Marks *et al.*, 2003; Grønnedal-Ika: Halama *et al.*, 2005). Therefore, comparing the T–f_{O2} conditions of the Motzfeldt rocks with those of other Gardar intrusions can reveal underlying mechanisms of alkaline to peralkaline magmatic differentiation (Fig. 14). The syenites in the Grønnedal-Ika complex crystallized at higher oxygen fugacities (~ΔFMQ +3 to +4; 700–900°C, Halama *et al.*, 2005) where only CO_2-bearing phases are stable (carbonates, cancrinite). In contrast, Markl *et al.* (2001) showed that the Ilímaussaq intrusion (the type locality of agpaitic rocks) crystallized under very reduced conditions (~ΔFMQ −3 to −4); consequently, the stable high-temperature fluid phase was methane-dominated (Krumrei *et al.*, 2007) and carbonates are absent at orthomagmatic conditions. Marks *et al.* (2003) showed that the granitic to syenitic Puklen intrusion crystallized at ~ΔFMQ ±0·0 to −2 and *c.* 800°C. Consequently, Puklen contains carbonate as a late-stage (alteration) product (Marks *et al.*, 2003). No evidence of CO_2 was found in the fluid inclusions (Köhler, 2004). However, in syenitic samples, which crystallized at oxygen fugacities of ΔFMQ −0·8 to −2·3 (Marks *et al.*, 2003), Köhler (2004) detected subordinate amounts of methane. In samples from the Puklen alkali granite, which formed at higher f_{O2}, only methane-free H_2O–NaCl fluid inclusions were observed. Grønnedal-Ika and Puklen lack any sign of agpaitic minerals such as eudialyte.

Globally, agpaitic rocks occur from early magmatic, as in the Ilímaussaq intrusion or Lovozero and Khibina (Kramm & Kogarko, 1994; Zaitsev *et al.*, 1998), to hydrothermal stages of crystallization (agpaitic pegmatites; e.g. in Langesundfjord, Tamazeght and Mont St. Hilaire; Brøgger, 1890; Bouabdli *et al.*, 1988; Horvath & Gault, 1990; Marks *et al.*, 2008). We propose that these differences may be related to the T–f_{O2} evolution of the respective intrusions. In this respect, it is interesting to note that in terms of f_{O2} evolution during magmatic differentiation, Motzfeldt is similar to but slightly more reduced than the Puklen intrusion; this may be related to the stronger contamination effects detected in the Puklen melts (Marks *et al.*, 2003). This slight change in redox (and crustal contamination) conditions to the more reducing side is just enough to allow the melt to enter the field of agpaitic mineral stability in the very last magmatic stage SM6. In the highly reduced Ilímaussaq intrusion, in contrast, eudialyte is found as an early crystallizing liquidus phase, which may be attributed to the reduced character.

This study demonstrates that fluid inclusion chemistry, particularly the speciation of a C–O–H fluid (CO_2 or CH_4), may serve as an excellent tracer for the redox conditions of the melt and help to understand the transition from miaskitic to agpaitic rocks. The transition from miaskitic to agpaitic rocks can be explained in terms of a continuous magmatic differentiation sequence in peralkaline systems. Several features are common to all agpaitic intrusions: (1) an extreme peralkaline composition, which causes the high solubility of trace elements such as Zr and other HFSE; these elements are complexed with Na and Si, forming the precursor species to the complex minerals of agpaitic rocks (eudialyte, rinkite); (2) an extremely long crystallization interval down to temperatures as low as 450°C; (3) redox reactions involving the speciation of Fe (Fe^{2+}/Fe^{3+}) and C (CO_2/CH_4); (4) no (or very late) exsolution of a characteristically methane-bearing fluid phase.

ACKNOWLEDGEMENTS

Adrian Finch, Ian Parsons and Julian Schilling are thanked for their help during the field work. Angus & Ross and their Greenland Team (especially Ashlyn Armour-Brown and Jamie McCreath) are thanked for the pleasant time in the field as well as giving the possibility to carry out a second field season. Henry Emeleus kindly provided one sample of SM2. Valuable discussions with Adrian Finch, Ian Parsons, Wolfgang Siebel, Heiner Taubald and Thomas Wagner helped to improve the interpretations of this study. Ralf Halama is thanked for his help with the calculations of the CO_2–CH_4 reaction curves, and Verena Krasz for carefully hand picking the mineral separates. Thomas Wenzel provided assistance with microprobe measurements, which is gratefully acknowledged. Gabi Stoschek, Bernd Steinhilber and Elmar Reitter are thanked for their help with the isotope analysis. Jasmin Köhler's help to improve an earlier version of this manuscript is gratefully acknowledged. The careful reviews and suggestions of Tom Andersen, Stefano Salvi and an anonymous reviewer and the editorial handling of Marjorie Wilson helped to improve the manuscript significantly. Financial support was provided by the German Science Foundation.

REFERENCES

Andersen, D. J. & Lindsley, D. H. (1985). New (and final!) models for the Ti-magnetite/ilmenite geothermometer and oxygen barometer. Abstracts, AGU 1985 Spring Meeting. *EOS Transactions, American Geophysical Union* **66**, 416 .

Andersen, D. J., Lindsley, D. H. & Davidson, P. M. (1993). QUILF; a Pascal program to assess equilibria among Fe–Mg–Mn–Ti oxides, pyroxenes, olivine, and quartz. *Computers and Geosciences* **19**, 1333–1350.

Armour-Brown, A., Tukiainen, T., Wallin, B., Bradshaw, C. & Emeleus, C. H. (1983). Uranium exploration in South Greenland. *Grønlands Geologiske Undersøgelse Rapport* **115**, 68–75.

Armstrong, J. T. (1991). Quantitative elemental analysis of individual microparticles with electron beam instruments. In: Heinrich, K. F. J. & Newbury, D. E. (eds) *Electron Probe Quantitation*. New York: Plenum, pp. 261–315.

Bakker, R. J. (2003). Package FLUIDS 1. Computer programs for analysis of fluid inclusion data and for modelling bulk fluid properties. *Chemical Geology* **194**, 3–23.

Beeskow, B., Treloar, P. J., Rankin, A. H., Vennemann, T. W. & Spangenberg, J. (2006). A reassessment of models for hydrocarbons generation in the Khibiny nepheline syenite complex, Kola Peninsula, Russia. *Lithos* **91**, 1–18.

Bezos, A. & Humler, E. (2005). The Fe^{3+}/Fe ratios of MORB glasses and their implications for mantle melting. *Geochimica et Cosmochimica Acta* **69**, 711–725.

Bodnar, R. J. (1993). Revised equation and table for determining the freezing point depression of the H_2O–NaCl solutions. *Geochimica et Cosmochimica Acta* **57**, 683–684.

Borovikov, A. A., Gushchina, L. N. & Borisekno, A. S. (2001). Specific features of $FeCl_2$ and $FeCl_3$ solution behaviour at low temperatures (cryometry of fluid inclusions). *XVI ECROFI European Current Research on Fluid Inclusions. Faculdade de Ciências do Porto, Departamento de Geologia, Memória* **7**, 61–63.

Bottomley, D. J., Gregoire, D. C. & Raven, K. G. (1994). Saline groundwaters and brines in the Canadian Shield: geochemical and isotopic evidence for a residual evaporite brine component. *Geochimica et Cosmochimica Acta* **58**, 1483–1498.

Bouabdli, A., Dupuy, C. & Dostal, J. (1988). Geochemistry of Mesozoic alkaline lamprophyres and related rocks from the Tamezeght massif, High Atlas, Morocco. *Lithos* **22**, 43–58.

Bradshaw, C. (1988). A petrographic, structural and geochemical study of the alkaline igneous rocks of the Motzfeldt centre, South Greenland. Ph.D. thesis, University of Durham.

Brøgger, W. V. (1890). Die Mineralien der Syenitpegmatitgänge der Südnorwegischen Augit- und Nephelinsyenite. *Zeitschrift für Kristallographie–Mineralogie* **16**, 1–663.

Brown, W. L. & Parsons, I. (1989). Alkali feldspars: ordering rates, phase transformations and behaviour diagrams for igneous rocks. *Mineralogical Magazine* **53**, 25–42.

Bureau, H. & Métrich, N. (2003). An experimental study of bromine behaviour in water-saturated silicic melts. *Geochimica et Cosmochimica Acta* **67**, 1689–1697.

Bureau, H., Keppler, H. & Métrich, N. (2000). Volcanic degassing of bromine and iodine: experimental fluid/melt partitioning data and applications to stratospheric chemistry. *Earth and Planetary Science Letters* **183**, 51–60.

Byers, C. D., Christie, D. M., Muenow, D. W. & Sinton, J. M. (1984). Volatile contents and ferric–ferrous ratios of basalt, ferrobasalt, andesite and rhyodacite glasses from the Galapagos 95·5°W propagating rift. *Geochimica et Cosmochimica Acta* **48**, 2239–2245.

Cartwright, I., Weaver, T., Tweed, S., Ahearne, D., Cooper, M., Czapnik, C. & Tranter, J. (2000). O, H, C isotope geochemistry of carbonated mineral springs in central Victoria, Australia: sources of gas and water–rock interaction during dying basaltic volcanism. *Journal of Geochemical Exploration* **69–70**, 257–261.

Chakhmouradian, A. R. & Mitchell, R. H. (2002). The mineralogy of Ba- and Zr-rich alkaline pegmatites from Gordon Butte, Crazy Mountains (Montana, USA): comparisons between potassic and sodic agpaitic pegmatites. *Contributions to Mineralogy and Petrology* **143**, 93–114.

Clarke, L. B., Le Bas, M. J. & Spiro, B. (1993). Rare earth, trace elements and stable isotope fractionation of carbonatites at Kruidfontein, Transvaal, South Africa. In: Meyer, H. O. A. & Leonardos, O. H. (eds) *Proceedings of the 5th Kimberlite Conference, 1, Kimberlite, Related Rocks and Mantle Xenoliths*. Brasilia: CPRM, pp. 236–251.

Coulson, I. M. (1997). Post-magmatic alteration in eudialyte from the North Qoroq centre, South Greenland. *Mineralogical Magazine* **61**, 99–109.

Coulson, I. M., Goodenough, K. M., Pearce, N. J. G. & Leng, M. J. (2003). Carbonatites and lamprophyres of the Gardar Province—a 'window' to the Sub-Gardar Mantle? *Mineralogical Magazine* **67**, 855–872.

Craig, H. (1961). Isotopic variations in meteoric waters. *Science* **133**, 1702.

Dallai, L., Ghezzo, C. & Sharp, Z. D. (2003). Oxygen isotope evidence for crustal assimilation and magma mixing in the Granite Harbour intrusives, Northern Victoria Land, Antarctica. *Lithos* **67**, 135–151.

Davis, W. D., Lowenstein, T. K. & Spencer, R. J. (1989). Melting behaviour of fluid inclusions in laboratory-grown halite crystals in the systems NaCl–H_2O, NaCl–KCl–H_2O, NaCl–$MgCl_2$–H_2O and NaCl–$CaCl_2$–H_2O. *Geochimica et Cosmochimica Acta* **54**, 591–601.

Deines, P. (1989). Stable isotope variations in carbonatites. In: Bell, K. (ed.) *Carbonatites: Genesis and Evolution*. London: Unwin Hyman, pp. 301–359.

Deméney, A., Ahijado, A., Casillas, R. & Vennemann, T. W. (1998). Crustal contamination and fluid/rock interaction in the carbonatites of Fuerteventura (Canary Islands, Spain): a C, O, H isotope study. *Lithos* **44**, 101–115.

DePaolo, D. J. (1981). Neodymium isotopes in the Colorado Front Range and crust–mantle evolution in the Proterozoic. *Nature* **291**, 193–196.

Des Marais, D. J. & Moore, J. G. (1984). Carbon and its isotopes in mid-oceanic basalt glasses. *Earth and Planetary Science Letters* **69**, 43–57.

Eiler, J. M. (2001). Oxygen isotope variations of basaltic lavas and upper mantle rocks. In: Valley, J. W. & Cole, D. R. (eds) *Stable Isotope Geochemistry. Mineralogical Society of America, Reviews in Mineralogy* **43**, 319–364.

Eiler, J. M., Schiano, P., Kitchen, N. & Stolper, E. M. (2000). Oxygen-isotope evidence for recycled crust in the sources of mid-ocean-ridge basalts. *Nature* **403**, 530–534.

Emeleus, C. H. & Harry, W. T. (1970). *The Igaliko Nepheline Syenite Complex; General Description. Meddelelser om Grønland* **186**, 115 pp.

Escher, A. & Watt, W. S. (1970). *Geology of Greenland*. Copenhagen: Geological Survey of Greenland, 603 pp.

Farges, F., Ponader, C. W. & Brown, G. E., Jr (1991). Structural environments of incompatible elements in silicate glass/melts systems, I. Zr at trace levels. *Geochimica et Cosmochimica Acta* **55**, 1563–1574.

Frape, S. K. & Fritz, P. (1982). The chemistry and isotopic composition of saline groundwaters from the Sudbury Basin, Ontario. *Canadian Journal of Earth Sciences* **19**, 645–661.

Frape, S. K., Fritz, P. & McNutt, R. H. (1984). Water–rock interaction and chemistry of groundwaters from the Canadian Shield. *Geochimica et Cosmochimica Acta* **48**, 1617–1627.

Friedman, I. (1953). Deuterium content of natural waters and other substances. *Geochimica et Cosmochimica Acta* **4**, 89–103.

Friedman, I. & O'Neil, J. R. (1977). Compilation of stable isotope fractionation factors of geochemical interest. In: Fleischer, M. (ed.) *Data of Geochemistry. US Geological Survey Professional Papers* **440-KK**, 12.

Frost, B. R. & Lindsley, D. H. (1992). Equilibria among Fe–Ti-oxides, pyroxenes, olivine, and quartz: Part II. Application. *American Mineralogist* **77**, 1004–1020.

Garde, A. A., Hamilton, M. A., Chadwick, B., Grocott, J. & McGaffrey, K. J. W. (2002). The Ketilidian orogen of South Greenland: geochronology, tectonics, magmatism, and fore arc accretion during Palaeoproterozoic oblique convergence. *Canadian Journal of Earth Sciences* **39**, 765–793.

Gerlach, S., Claußen, O. & Rüssel, C. (1998). Thermodynamics of iron in alkali–magnesia–silica glasses. *Journal of Non-Crystalline Solids* **238**, 75–82.

Gerlach, S., Claußen, O. & Rüssel, C. (1999). A voltammetric study on the thermodynamics of the Fe^{3+}/Fe^{2+}-equilibrium in alkali–lime–alumosilicate melts. *Journal of Non-Crystalline Solids* **248**, 92–98.

Goldstein, S. L., O'Nions, R. K. & Hamilton, P. J. (1984). A Sm–Nd isotopic study of the atmospheric dust and particulates from major river systems. *Earth and Planetary Science Letters* **70**, 221–236.

Goodenough, K. M. (1997). Geochemistry of Gardar intrusions in the Ivigtut Area, South Greenland. Ph.D. thesis, University of Edinburgh.

Graham, C. M., Harmon, R. S. & Sheppard, S. M. F. (1984). Experimental hydrogen isotope studies: hydrogen isotope exchange between amphibole and water. *American Mineralogist* **69**, 128–138.

Graser, G., Potter, J., Köhler, J. & Markl, G. (in press). Isotope, major, minor and trace element geochemistry of late-magmatic fluids in the peralkaline Ilímaussaq intrusion, South Greenland. *Lithos*, doi: 10.1016/j.lithos.2008.07.007.

Halama, R., Wenzel, T., Upton, B. G. J., Siebel, W. & Markl, G. (2003). A geochemical and Sr–Nd–O isotopic study of the Proterozoic Eriksfjord Basalts, Gardar Province, South Greenland: Reconstruction of an OIB signature in crustally contaminated rift-related basalts. *Mineralogical Magazine* **67**, 831–854.

Halama, R., Vennemann, T., Siebel, W. & Markl, G. (2005). The Grønnedal-Ika carbonatite–syenite complex, South Greenland: An origin involving liquid immiscibility. *Journal of Petrology* **46**, 191–217.

Hamilton, D. L. (1961). Nephelines as crystallisation temperature indicators. *Journal of Geology* **69**, 321–329.

Hanchar, J. M. & Watson, E. B. (2003). Zircon saturation thermometry. In: Hanchar, J. M. & Hoskin, P. W. O. (eds) *Zircon. Mineralogical Society of America, Reviews in Mineralogy and Geochemistry* **53**, 89–112.

Harris, C. (1995). Oxygen isotope geochemistry of the Mesozoic anorogenic complexes of Damaraland, northwest Namibia: evidence for crustal contamination and its effects on silica saturation. *Contributions to Mineralogy and Petrology* **122**, 308–321.

Hoefs, J. (1997). *Stable Isotope Geochemistry*. Berlin: Springer.

Hollemann, A. F. & Wiberg, E. (1995). *Lehrbuch der anorganischen Chemie*. Berlin: De Gruyter, 101 pp.

Horvath, L. & Gault, R. A. (1990). The mineralogy of Mont Saint-Hilaire, Quebec. *Mineralogical Record* **21**, 284–359.

Hoskin, P. W. O. & Schaltegger, U. (2003). The composition of zircon and igneous and metamorphic petrogenesis. In: Hanchar, J. M. & Hoskin, P. W. O. (eds) *Zircon. Mineralogical Society of America, Reviews in Mineralogy and Geochemistry* **53**, 27–62.

Huizenga, J. M. (2001). Thermodynamic modelling of C–O–H fluids. *Lithos* **55**, 101–114.

Huizenga, J. M. (2005). COH, an Excel spreadsheet for composition calculations in the C–O–H fluid system. *Computers and Geosciences* **31**, 797–800.

Jacobson, S. B. & Wasserburg, G. J. (1980). Sm–Nd isotopic evolution of chondrites. *Earth and Planetary Science Letters* **50**, 139–155.

Jones, A. P. (1980). Petrology and structure of the Motzfeldt centre, Igaliko complex, South Greenland. Ph.D. thesis, University of Durham.

Jones, A. P. (1984). Mafic silicates from the nepheline syenites of the Motzfeldt centre, south Greenland. *Mineralogical Magazine* **48**, 1–12.

Jones, A. P. & Larsen, L. M. (1985). Geochemistry and REE minerals of nepheline syenites from the Motzfeldt Centre, South Greenland. *American Mineralogist* **70**, 1087–1100.

Jones, A. P. & Peckett, A. (1980). Zirconium-bearing aegirines from Motzfeldt, South Greenland. *Contributions to Mineralogy and Petrology* **75**, 251–255.

Keller, J. & Hoefs, J. (1995). Stable isotope characteristics of recent natrocarbonatites from Oldoinyo Lengai. In: Bell, K. & Keller, J. (eds) *Carbonatite Volcanism: Oldoinyo Lengai and the Petrogenesis of Natrocarbonatites*. Berlin: Springer, pp. 113–123.

Kelly, W. C., Rye, R. O. & Livnat, A. (1986). Saline minewaters of the Keweenaw Peninsula, Northern Michigan: Their natural origin and relation to similar deep waters in the Precambrian crystalline rocks of the Canadian Shield. *American Journal of Science* **286**, 281–308.

Khomyakov, A. P. (1995). *Mineralogy of Hyperagpaitic Alkaline Rocks*. Oxford: Oxford Science Publications, Clarendon Press.

Kilinc, A., Carmichael, I. S. E., Rivers, M. L. & Sack, R. O. (1983). The ferric–ferrous ratio of natural silicate liquids equilibrated in air. *Contributions to Mineralogy and Petrology* **83**, 136–141.

Kogarko, L. N. (1974). Rôle of volatiles. In: Sørensen, H. (ed.) *The Alkaline Rocks*. London: John Wiley, pp. 474–487.

Kogarko, L. N. (1987). Alkaline rocks of the eastern part of the Baltic Shield (Kola Peninsula). In: Fitton, J. G. & Upton, B. G. J. (eds) *Alkaline Igneous Rocks. Geological Society, London, Special Publications* **30**, 531–544.

Kogarko, L. N. & Romanchev, B. P. (1983). Phase equilibria in alkaline melts. *International Geological Reviews* **25**, 534–546.

Kogarko, L. N., Burnham, C. W. & Shettle, D. (1977). Water regime in alkalic magmas. *Geochemistry International* **14**, 1–8.

Kogarko, L. N., Kosztolanyi, C. & Ryabchikov, I. D. (1987). Geochemistry of the reduced fluid in alkali magmas. *Geochemistry International* **24**, 20–27.

Köhler, J. (2004). Petrologische und Geochemische Untersuchungen von Fluideinschlüssen in Gesteinen der Puklen Intrusion, Südgrönland. Masters thesis, University of Tübingen.

Köhler, J., Konnerup-Madsen, J. & Markl, G. (2008). Fluid chemistry in the Ivigtut cryolite deposit, South Greenland. *Lithos* **103**, 369–392.

Konnerup-Madsen, J. (2001). A review of the composition and evolution of hydrocarbon gases during solidification of the Ilímaussaq alkaline complex, South Greenland. *Geology of Greenland Survey Bulletin* **301**, 159–166.

Konnerup-Madsen, J. & Rose-Hansen, J. (1982). Volatiles associated with alkaline igneous rift activity: fluid inclusions in the Ilímaussaq intrusion and the Gardar granite complexes. *Chemical Geology* **37**, 79–93.

Konnerup-Madsen, J. & Rose-Hansen, J. (1984). Composition and significance of fluid inclusions in the Ilímaussaq peralkaline granite, South Greenland. *Bulletin de Minéralogie* **107**, 317–326.

Konnerup-Madsen, J., Dubessy, J. & Rose-Hansen, J. (1985). Combined Raman microprobe spectrometry and microthermometry of fluid inclusions in minerals from igneous rocks of the Gardar province (south Greenland). *Lithos* **18**, 271–280.

Kramm, U. & Kogarko, L. N. (1994). Nd and Sr isotope signatures of the Khibina and Lovozero agpaitic centres, Kola Province, Russia. *Lithos* **32**, 225–242.

Kress, V. C. & Carmichael, I. S. E. (1988). Stoichiometry of the iron oxidation reaction in silicate melts. *American Mineralogist* **73**, 1267–1274.

Kress, V. C. & Carmichael, I. S. E. (1989). The lime–iron–silicate melt system: Redox and volume systematics. *Geochimica et Cosmochimica Acta* **53**, 2883–2892.

Kress, V. C. & Carmichael, I. S. E. (1991). The compressibility of silicate liquids containing Fe_2O_3 and the effect of composition, temperature, oxygen fugacity and pressure on their redox states. *Contributions to Mineralogy and Petrology* **198**, 82–92.

Krumrei, T., Kaliwoda, M., Pernicka, E. & Markl, G. (2007). Volatiles in a peralkaline system: Abiogenic hydrocarbons and F–Cl–Br systematics in the naujaite of the Ilimaussaq intrusion, South Greenland. *Lithos* **95**, 298–314.

Kyser, T. K. (1986). Stable isotope variations in the mantle. In: Valley, J. W., Taylor, H. P. & O'Neil, J. R. (eds) *Stable Isotopes in High Temperature Geological Processes. Mineralogical Society of America, Reviews in Mineralogy* **16**, 141–164.

Kyser, T. K., O'Neil, J. R. & Carmichael, I. S. E. (1982). Genetic relations among basic lavas and ultramafic nodules: evidence from oxygen isotope compositions. *Contributions to Mineralogy and Petrology* **81**, 88–102.

Lange, R. A. & Carmichael, I. S. E. (1989). Ferric–ferrous equilibria in Na_2O–FeO–Fe_2O_3–SiO_2 melts: Effects of analytical techniques on derived partial molar volumes. *Geochimica et Cosmochimica Acta* **53**, 2195–2204.

Larsen, L. M. & Sørensen, H. (1987). The Ilímaussaq intrusion—progressive crystallization and formation of layering in an agpaitic magma. In: Fitton, J. G. & Upton, B. G. J. (eds) *Alkaline Igneous Rocks. Geological Society, London, Special Publications* **30**, 473–488.

Leake, B. E., (Chairman) (1997). Nomenclature of amphiboles. Report of the Subcommittee on Amphiboles of the International Mineralogical Association Commission on New Minerals and Mineral Names. *European Journal of Mineralogy* **9**, 623–651.

Lepage, L. D. (2003). ILMAT: an Excel worksheet for ilmenite–magnetite geothermometry and geobarometry. *Computers and Geosciences* **29**, 673–678.

Liew, T. C. & Hofmann, A. W. (1987). Precambrian crustal components, plutonic associations, plate environment of the Hercynian Fold Belt of central Europe: Indications from a Nd and Sr isotopic study. *Contributions to Mineralogy and Petrology* **98**, 129–138.

Lindsley, D. H. & Frost, B. R. (1992). Equilibria among Fe–Ti-oxides, pyroxenes, olivine, and quartz: Part I. Theory. *American Mineralogist* **77**, 987–1003.

Lugmair, G. W. & Marti, K. (1978). Lunar initial $^{143}Nd/^{144}Nd$: differential evolution of the lunar crust and mantle. *Earth and Planetary Science Letters* **39**, 349–357.

Markl, G. (2001). A new type of silicate liquid immiscibility macroscopically visible in Proterozoic peralkaline rocks from Ilímaussaq, South Greenland. *Contributions to Mineralogy and Petrology* **141**, 458–472.

Markl, G. & Baumgartner, L. (2002). pH changes in peralkaline late-magmatic fluids. *Contributions to Mineralogy and Petrology* **144**, 331–346.

Marks, M. & Markl, G. (2001). Fractionation and assimilation processes in the alkaline augite syenite unit of the Ilimaussaq Intrusion, South Greenland, as deduced from phase equilibria. *Journal of Petrology* **42**, 1947–1969.

Markl, G., Marks, M., Schwinn, G. & Sommer, H. (2001). Phase equilibrium constraints on intensive crystallization parameters of the Ilímaussaq Complex, South Greenland. *Journal of Petrology* **42**, 2231–2258.

Marks, M., Vennemann, T., Siebel, W. & Markl, G. (2003). Quantification of magmatic and hydrothermal processes in a peralkaline syenite–alkali granite complex based on textures, phase equilibria, and stable and radiogenic isotopes. *Journal of Petrology* **44**, 1247–1280.

Marks, M., Venemann, T., Siebel, W. & Markl, G. (2004). Nd-, O-, and H-isotopic evidence for complex, closed-system fluid evolution of the peralkaline Ilímaussaq intrusion, South Greenland. *Geochimica et Cosmochimica Acta* **68**, 3379–3395.

Marks, M., Rudnick, R. L., McCammon, C., Vennemann, T. & Markl, G. (2007). Arrested kinetic Li isotopic fractionation at the margin of the Ilímaussaq complex, South Greenland: evidence for open-system processes during final cooling of peralkaline igneous rocks. *Chemical Geology* **246**, 207–230.

Marks, M., Schilling, J., Coulson, I., Wenzel, T. & Markl, G. (2008). The alkaline–peralkaline Tamazeght Complex, High Atlas Mountains, Morocco: mineral chemistry and petrological constraints for derivation from a compositionally heterogeneous mantle source. *Journal of Petrology* **49.**

McDowell, S. D. (1986). Composition and structural state of coexisting feldspars, Salton Sea geothermal field. *Mineralogical Magazine* **50**, 75–84.

Mitchell, R. H. & Liferovich, R. P. (2006). Subsolidus deuteric/hydrothermal alteration of eudialyte in lujavrite from the Pilansberg alkaline complex, South Africa. *Lithos* **91**, 352–372.

Nicholls, J. & Carmichael, I. S. E. (1969). Peralkaline acid liquids: a petrological study. *Contributions to Mineralogy and Petrology* **20**, 268–294.

Nielsen, T. F. D. (1994). Alkaline dike swarms of the Gardiner complex and the origin of ultramafic alkaline complexes. *Geochemistry International* **31**, 37–56.

Nivin, V. A., Belov, N. I., Treloar, P. J. & Timofeyev, V. V. (2001). Relationships between gas geochemistry and release rates and the geochemical state of igneous rock massifs. *Tectonophysics* **336**, 233–244.

Nivin, V. A., Ikorskii, S. V. & Treloar, P. J. (2002). Bulk gas content variations in fluid inclusions of minerals from the Khibina and Lovozero nepheline-syenite plutons (NE Baltic Shield, Russia); implication for origin of hydrocarbon gases. *Abstracts of the 18th General Meeting of the International Mineralogical Association* **18**, 248 .

Nivin, V. A., Treloar, P. J., Konopleva, N. G. & Ikorsky, S. V. (2005). A review of the occurrence, form and origin of C-bearing species in the Khibiny alkaline igeneous complex, Kola Peninsula, NW Russia. *Lithos* **85**, 93–112.

Ohmoto, H. & Goldhaber, M. B. (1997). Sulfur and carbon isotopes. In: Barnes, H. L. (ed.) *Geochemistry of Hydrothermal Ore Deposits*, 3rd edn. New York: John Wiley, pp. 517–611.

Pearce, N. J. G. & Leng, M. J. (1996). The origin of carbonatites and related rocks from the Igaliko Dyke Swarm, Gardar Province, South Greenland: field, geochemical and C–O–Sr–Nd isotope evidence. *Lithos* **39**, 21–40.

Pearce, N. J. G., Leng, M. J., Emeleus, C. H. & Bedford, C. M. (1997). The origins of carbonatites and related rocks from the Grønnedal-Ika Nepheline Syenite Complex, South Greenland: C–O–Sr isotope evidence. *Mineralogical Magazine* **61**, 515–529.

Petersilie, I. A. & Sørensen, H. (1970). Hydrocarbon gases and bituminous substances in rocks from the Ilímaussaq alkaline intrusion, South Greenland. *Lithos* **3**, 59–76.

Pineau, F. & Javoy, M. (1983). Carbon isotopes and concentrations in mid-oceanic ridge basalts. *Earth and Planetary Science Letters* **62**, 239–257.

Piotrowski, J. M. & Edgar, A. D. (1970). Melting relations of undersaturated alkaline rocks from South Greenland compared to those of Africa and Canada. *Meddelelser om Grønland* **181.**

Potter, J. & Konnerup-Madsen, J. (2003). A review of the occurrence and origin of abiogenic hydrocarbons in igneous rocks. In: Petford, N. & McCaffrey, K. J. W. (eds) *Hydrocarbons in Crystalline Rocks. Geological Society, London, Special Publications* **214**, 151–173.

Potter, J., Rankin, A. H. & Treloar, P. J. (1999). The relationship between CH_4 and CO_2 inclusions and Fe–O–S mineralization in intrusions of the Kola Alkaline Province. In: Stanley, C. J. *et al.* (eds) *Mineral Deposits: Processes to Processing 1.* Rotterdam: Balkema, pp. 87–90.

Potter, J., Rankin, A. H. & Treloar, P. J. (2004). Abiogenic Fischer-Tropsch synthesis of hydrocarbons in alkaline igneous rocks; fluid inclusion, textural and isotopic evidence from the Lovozero Complex, N.W. Russia. *Lithos* **75**, 311–330.

Richet, P., Bottinga, Y. & Javoy, A. (1977). A review of hydrogen, carbon, nitrogen, oxygen, sulphur and chlorine stable isotope fractionation among gaseous molecules. *Annual Review of Earth and Planetary Sciences* **5**, 65–110.

Robie, R. A. & Hemingway, B. S. (1995). *Thermodynamic properties of minerals and related substances at 298.15 K and 1 bar (105 Pascals) pressure and at higher temperatures. US Geological Survey, Bulletin* **2131**, 461 pp.

Rumble, D. & Hoering, T. C. (1994). Analysis of oxygen and sulfur isotope ratios in oxide and sulfide minerals by spot heating with a carbon dioxide laser in a fluorine atmosphrere. *Accounts of Chemical Research* **27**, 237–241.

Rüssel, C. & Wiedenroth, A. (2004). The effect of glass composition on the thermodynamics of the Fe^{2+}/Fe^{3+} equilibrium and the iron diffusivity in $Na_2O/MgO/CaO/Al_2O_3/SiO_2$ melts. *Chemical Geology* **213**, 125–135.

Ryabchikov, I. D. & Kogarko, L. N. (2006). Magnetite compositions and oxygen fugacities of the Khibina magmatic system. *Lithos* **91**, 35–45.

Sack, R. O., Carmichael, I. S. E., Rivers, M. & Ghiorso, M.S. (1981). Ferric–ferrous equilibria in natural silicate liquids at 1 bar. *Contributions to Mineralogy and Petrology* **75**, 369–377.

Salvi, S. & Williams-Jones, A. E. (1990). The role of hydrothermal processes in the granite hosted Zr, Y, REE deposit at Strange Lake, Quebec/Labrador: evidence from fluid inclusions. *Geochimica et Cosmochimica Acta* **54**, 2403–2418.

Salvi, S. & Williams-Jones, A. E. (1997). Fischer-Tropsch synthesis of hydrocarbons during sub-solidus alteration of the Strange Lake peralkaline granite, Quebec/Labrador, Canada. *Geochimica et Cosmochimica Acta* **61**, 83–99.

Salvi, S. & Williams-Jones, A. E. (2006). Alteration, HFSE mineralisation and hydrocarbon formation in peralkaline igneous systems: Insights from the Strang Lake Pluton, Canada. *Lithos* **91**, 19–34.

Schoell, M. (1988). Multiple origins of methane in the Earth. *Chemical Geology* **71**, 1–10.

Schönenberger, J., Marks, M., Wagner, T. & Markl, G. (2006). Fluid–rock interaction in autoliths of agpaitic nepheline syenites in the Ilimaussaq intrusion, South Greenland. *Lithos* **91**, 331–351.

Schönenberger, J., Köhler, J. & Markl, G. (2008). REE systematics of fluorides, calcite and siderite in peralkaline plutonic rocks from the Gardar Province, South Greenland. *Chemical Geology* **247**, 16–37.

Sharp, Z. D. (1990). A laser-based microanalytical method for the in-situ determination of oxygen isotope ratios of silicates and oxides. *Geochimica et Cosmochimica Acta* **54**, 1353–1357.

Shepherd, T. J., Rankin, A. H. & Alderton, D. H. M. (1985). *A Practical Guide to Fluid Inclusion Studies*. Glasgow: Blackie.

Sheppard, S. M. F. (1986). Characterization and isotopic variations in natural waters. In: Valley, J. W., Taylor, H. P., Jr & O'Neil, J. R. (eds) *Stable Isotopes. Mineralogical Society of America, Reviews in Mineralogy* **16**, 165–181.

Sheppard, S. M. F. (1989). The isotopic characterization of aqueous and leucogranitic crustal fluids. *NATO ASI Series, Series C: Mathematical and Physical Sciences* **281**, 245–263.

Shi, P. & Saxena, S. K. (1992). Thermodynamic modelling of the C–O–H–S fluid system. *American Mineralogist* **77**, 1038–1044.

Sood, M. K. & Edgar, A. D. (1970). Melting relations of undersaturated alkaline rocks from the Ilímaussaq intrusion and Grønnedal-Ìka complex South Greenland, under water vapour and controlled partial oxygen pressure. *Meddelelser om Grønland* **181.**

Sørensen, H. (1997). The agpaitic rocks—an overview. *Mineralogical Magazine* **61**, 485–498.

Spötl, C. & Vennemann, T. W. (2003). Continuous-flow isotope ratio mass spectrometric analysis of carbonate minerals. *Rapid Communications in Mass Spectrometry* **17**, 1004–1006.

Suzuoki, T. & Epstein, S. (1976). Hydrogen isotope fractionation between OH-bearing minerals and water. *Geochimica et Cosmochimica Acta* **40**, 1229–1240.

Taubald, H., Morteani, G. & Satir, M. (2004). Geochemical and isotopic (Sr, C, O) data from the alkaline complex of Grønnedal-Ika (South Greenland): evidence for unmixing and crustal contamination. *International Journal of Earth Sciences* **93**, 348–360.

Taylor, H. P. (1974). The application of oxygen and hydrogen isotope studies to problems of hydrothermal alteration and ore deposition. *Economic Geology* **69**, 843–883.

Taylor, H. P. (1977). Water/rock interactions and the origin of H_2O in granitic batholiths. *Journal of the Geological Society, London* **133**, 509–558.

Taylor, H. P., Frechen, J. & Degens, E. T. (1967). Oxygen and carbon isotope studies of carbonatites from the Laacher See District, West Germany and the Aln€o District, Sweden. *Geochimica et Cosmochimica Acta* **31**, 407–430.

Taylor, H. P., Jr & Sheppard, S. M. F. (1986). Igneous rocks: I. Processes of isotopic fractionation and isotope systematics. In: Valley, J. W., Taylor, H. P., Jr & O'Neil, J. R. (eds) *Stable Isotopes. Mineralogical Society of America, Reviews in Mineralogy* **16**, 227–269.

Taylor, R. P., Strong, D. F. & Fryer, B. J. (1981). Volatile control of contrasting trace element distributions in peralkaline granitic and volcanic rocks. *Contributions to Mineralogy and Petrology* **77**, 267–271.

Tichomirowa, M., Grosche, G., Götze, J., Belyatsky, B. V., Savva, E. V., Keller, J. & Todt, W. (2006). The mineral isotope composition of two Precambrian carbonatite complexes from the Kola Alkaline Province—Alteration versus primary magmatic signatures. *Lithos* **91**, 229–249.

Treuil, M., Joron, J. L., Jaffrezic, H., Villemant, B. & Calas, G. (1979). Géochimie des elements hygromagmatophiles: Coefficients de partage minéraux/liquides et propriétés structurales de ces éléments dans les liquides magmatiques. *Bullétin de Mineralogie* **102**, 402–409.

Tukiainen, T., Bradshaw, C. & Emeleus, C. H. (1984). Geological and radiometric mapping of the Motzfeldt Centre of the Igaliko Complex, South Greenland. *Grønlands Geologiske Undersøgelse* **120**, 78–83.

Tuttle, O. F. & Bowen, N. L. (1958). *Origin of Granite in the Light of Experimental Studies in the System $NaAlSi_3O_8$–$KAlSi_3O_8$–SiO_2–H_2O. Geological Society of America, Memoirs* **74**.

Upton, B. G. J. & Emeleus, C. H. (1987). Mid-Proterozoic alkaline magmatism in southern Greenland: the Gardar Province. In: Fitton, J. G. & Upton, B. G. J. (eds). *Alkaline Igneous Rocks. Geological Society, London, Special Publications* **30**, 449–471.

Upton, B. G. J., Emeleus, C. H., Heaman, L. M., Goodenough, K. M. & Finch, A. A. (2003). Magmatism of the mid-Proterozoic Gardar Province, South Greenland: chronology, petrogenesis and geological setting. *Lithos* **68**, 43–65.

Valley, J. W., Kitchen, N., Kohn, M. J., Niendorf, C. R. & Spicuzza, M. J. (1995). UWG-2, a garnet standard for oxygen isotope ratios: strategies for high precision and accuracy with laser heating. *Geochimica et Cosmochimica Acta* **59**, 5223–5231.

Vennemann, T. W. & O'Neil, J. R. (1993). A simple and inexpensive method of hydrogen isotope and water analyses of minerals and rocks based on zinc reagent. *Chemical Geology* **103**, 227–234.

Vitrac-Michard, A., Albarède, F. & Azambre, B. (1977). Age Rb–Sr et $^{39}Ar/^{40}Ar$ de la syénite néphélinique de Fitou (Corbières orientales). *Bullétin de la Societé Française de Minéralogie et Cristallographie* **100**, 251–254.

Wallace, G. M., Whalen, J. B. & Martin, R. F. (1990). Agpaitic and miaskitic nepheline syenites of the McGerricle plutonic Complex, Gaspé, Quebec: An unusual petrological association. *Canadian Mineralogist* **28**, 251–266.

Watson, E. B. (1979). Zircon saturation in felsic liquids: Experimental results and applications to trace element geochemistry. *Contributions to Mineralogy and Petrology* **70**, 407–419.

Watson, E. B. & Harrison, T. M. (1983). Zircon saturation revisited: temperature and composition effects in a variety of crustal magma types. *Earth and Planetary Science Letters* **64**, 295–304.

Wolff, J. A. (1987). Crystallization of nepheline syenite in a subvolcanic magma system: Tenerife, Canary Islands. *Lithos* **20**, 207–223.

Worley, B. A., Cooper, A. F. & Hall, C. E. (1995). Petrogenesis of carbonate-bearing nepheline syenites and carbonatites from Southern Victoria Land, Antarctica: origin of carbon and the effects of calcite–graphite equilibrium. *Lithos* **35**, 183–199.

Zaitsev, A. N., Wall, F. & LeBas, M. J. (1998). REE–Sr–Ba minerals from the Khibina carbonatites, Kola Peninsula, Russia; their mineralogy, paragenesis and evolution:. *Mineralogical Magazine* **62**, 225–250.

Zhao, Z. F. & Zheng, Y. F. (2003). Calculation of oxygen isotope fractionation in magmatic rocks. *Chemical Geology* **193**, 59–80.

Zheng, Y. G. (1993*a*). Calculation of oxygen isotope fractionation in anhydrous silicate minerals. *Geochimica et Cosmochimica Acta* **57**, 1079–1091.

Zheng, Y. F. (1993*b*). Calculation of oxygen isotope fractionation in hydroxyl-bearing silicates. *Earth and Planetary Science Letters* **120**, 247–263.

Zheng, Y. F. (1999). Oxygen isotope fractionation in carbonate and sulfate minerals. *Geochemical Journal* **33**, 109–126.